Journal of Electroceramics, 8, 5–36, 2002

Feature Article

$BaTiO_{3-\delta}$: Defect Structure, Electrical Conductivity, Chemical Diffusivity, Thermoelectric Power, and Oxygen Nonstoichiometry

HAN-ILL YOO, CHANG-ROCK SONG* & DOH-KWON LEE

Solid State Ionics Research Lab., School of Materials Science and Engineering, Seoul National University, Seoul 151-742, Korea

Submitted October 29, 2001; Revised February 13, 2002; Accepted February 19, 2002

Abstract. Electrical conductivity, thermoelectric power, and chemical diffusivity are the most typical, charge-and-mass transport properties of a mixed ionic electronic conductor oxide which are essentially governed by its defect structure, and the oxygen nonstoichiometry is a direct measure of its overall defect concentration. For the system of $BaTiO_{3-\delta}$, the total electrical conductivity has been the most extensively and systematically studied as a function of oxygen partial pressure at elevated temperatures. The other properties have also been studied, but much less extensively and systematically. The electrical conductivity and thermopower were occasionally measured together on the same specimens so that mutual compatibility or consistency might be secured. But, the rest were all determined separately on the specimens of differing quality, consequently lacking in mutual consistency. It, thus, has remained hard to evaluate the canonical, defect-chemical parameters which are consistent with each and every of these defect structure-sensitive properties that were observed. Very recently the authors have determined the total conductivity, chemical diffusivity and thermoelectric power altogether on the same specimens of $BaTiO_{3-\delta}$, and the nonstoichiometry on the same-quality specimens at temperatures of $1073 \leq T/K \leq 1373$ over wide enough a range of oxygen partial pressure (normally, $10^{-16} \leq P_{O_2}/\text{atm} \leq 1$) that encloses an electron/hole/ion mixed regime. In this article, we will compile all the literature data on these defect-structure-sensitive properties and extract from the authors' own, without using any ad hoc assumptions regarding, e.g., the electronic carrier mobilities and effective density of states, the basic defect-chemical parameters including defect-equilibrium constants, carrier mobilities and densities, and electronic heats of transport, which are the most consistent with the properties observed. Compared to the conventional picture of the defect structure of "undoped" $BaTiO_3$, thus, some new insights into the defect chemical nature of $BaTiO_{3-\delta}$ are provided.

Keywords: $BaTiO_3$, electrical conductivity, chemical diffusivity, thermoelectric power, oxygen nonstoichiometry, defect structure

1. Introduction

$BaTiO_{3-\delta}$ enjoys wide applications as a main substance in modern electroceramics and electronics, e.g., positive temperature coefficient resistors (PTCR) [1], multi-layer capacitors (MLCC) [2], dielectric memories (DRAM) [3], and ferroelectric memories (FRAM) [4], to name only a few. For all these applications, knowledge and control of its defect structure and mass-and-charge transport properties among others are essential to endow the oxide with necessary functions as well as to design and/or optimize the processing route of the devices thereof. In order to make a PTCR element, for example, the interior of $BaTiO_3$ grains should be made into *n*-type semiconducting by doping donors and grain boundaries into electrically insulating by oxidation [5]. The thickness of the latter should be carefully controlled for optimum PTCR performance by appropriately adjusting the oxygen nonstoichiometry during cooling after sintering. Another example may

*Present address: Hynix Semiconductor Inc., Korea.

be an MLCC employing base metal electrodes (e.g., Ni or Cu): it should be sintered in a reducing atmosphere to avoid oxidation of the base metal, while somehow suppressing the generation of electrons and oxygen vacancies in order to retard dielectric degradation during service of the devices.

From a defect chemical point of view, $BaTiO_{3-\delta}$ is a very interesting oxide. The oxide is a mixed ionic electronic conductor in a quite extended range of oxygen partial pressure (e.g., $-15 \leq \log P_{O_2}/\text{atm} \leq 0$ at 1000°C), in the middle of which a p-type to n-type transition occurs while an appreciable, ionic partial conductivity remains nearly independent of P_{O_2}. This sort of electron/hole/ion mixed conduction is quite rare in binary oxides. MnO and TiO_2 among others are reported to show a mixed n/p behavior [6–8], but these oxides are nearly totally electronic so that any ionic contribution is hardly seen. Furthermore, either an n-type (for MnO) or p-type (for TiO_2) region of P_{O_2} is so narrow that the n/p mixed behavior is hardly observed. In the system of $BaTiO_3$, however, one can see each and every aspect of mobile ions, electrons and holes altogether simultaneously. In this regard, $BaTiO_3$ may serve as an excellent prototype of perovskite oxides which are now finding a rich variety of electrochemical applications such as energy or information conversion or storage (e.g., solid oxide fuel cells, batteries and sensors).

The electrical conductivity, thermoelectric power, and diffusivity are the most typical, charge-and-mass transport properties which are essentially governed by the defect structure of a system, and the oxygen nonstoichiometry is a direct measure of overall defect concentration. For the system of $BaTiO_3$, the total electrical conductivity has been the most extensively and systematically studied against temperature and oxygen partial pressure. Thermoelectric power, chemical diffusivity, tracer diffusivities, and oxygen nonstoichiometry have also been studied, but much less extensively and systematically. Electrical conductivity and thermopower were occasionally measured together on the same specimens so that the mutual compatibility or consistency between these two properties might often be secured. But, the rest were all measured separately on specimens of differing quality, consequently lacking in mutual consistency or compatibility among these properties. It has, thus, been hard to evaluate the canonical, defect-chemical parameters which are consistent with each and every of these defect structure-sensitive properties that were observed.

Very recently, the present authors have determined the total conductivity (σ), chemical diffusivity ($\tilde{D}$), thermoelectric power (θ), and nonstoichiometry (δ) altogether on the identical-quality samples of $BaTiO_3$ in its apparent equilibrium state at elevated temperatures (normally, $1073 \leq T/K \leq 1373$), over wide enough a range of oxygen partial pressure (normally, $10^{-16} \leq P_{O_2}/\text{atm} \leq 1$), that encloses the n-to-p transition. [9–13] All the samples examined are polycrystalline $BaTiO_3$ that were sintered from the identical starting powder of 99.995% pure $BaTiO_3$ (Aldrich, Lot 05717BN) with no sintering aid (e.g. excess TiO_2) added at all. According to the manufacturer's product information, the powder bears only Fe, Si and Al as nonvolatile impurities by 5, 5 and 1 ppm, respectively. Nevertheless, their microstructural details differ somewhat: The first three properties (σ, $\tilde{D}$, θ) measured on the same samples with a relative density of $94 \pm 1\%$ and average grain size of 43 ± 8 μm; the last one (δ) on the ones with ca. 90% density and the average grain size of 60 ± 20 μm. (For experimental details, readers are referred to Ref. 9, 11–13.) Furthermore, for the comparison purpose, the same properties have been determined on single crystal $BaTiO_3$ which are intentionally doped with Al as acceptors (Al'_{Ti}) by 1.8 m/o [14]. One is now ready to draw a more consistent and collective picture of correlations among the defect structure and transport properties of undoped $BaTiO_3$.

This article is organized as follows. In Section 2, we summarize the defect structures of "undoped" and acceptor-doped $BaTiO_3$, which are apparently consistent with all the charge-and-mass transport properties that have been observed experimentally. In the immediately following four sections, we will discuss the electrical conductivity (Section 3), the chemical diffusivity (Section 4), the thermoelectric power (Section 5), and the nonstoichiometry (Section 6), in turn. Each section starts with compilation of all the literature data including the authors' own on the property under consideration. It follows that the property is correlated to the defect structure and the authors' own data are subsequently analyzed in view of this correlation with a focus upon the electron/hole/ion mixed regime. When necessary to make the connotation clearer, we compare the results from the "undoped" with those from the Al-doped single crystal. Finally in Section 7, we present the correlation between each of the transport properties and the nonstoichiometry, and close with a few concluding remarks.

2. Defect Structure

Defect structure of $BaTiO_{3-\delta}$ has been estimated to date mostly from the total-conductivity variation against oxygen partial pressure at elevated temperatures, which is discussed in detail in Section 3. Regarding the defect structure, a consensus seems to have been reached for "undoped" and acceptor-doped $BaTiO_3$, unlike donor-doped $BaTiO_3$ where charge compensation mechanisms are still under controversy [15]. In this section, we summarize the possible defect structures of "undoped" $BaTiO_3$. Here we mean by "undoped" that the oxide is not-intentionally doped, but may contain background impurities which, if any, are of acceptor-type as will be clear in Section 3.

The irregular structure elements in the "undoped" $BaTiO_3$ may then be electrons (e'), holes ($h^\bullet$), oxygen vacancies ($V_O^{\bullet\bullet}$), cation vacancies (V''_{Ba} and V''''_{Ti}) and acceptor-type impurities (A'_C). The possibility of interstitial disorders is ruled out from a structural viewpoint [16–18]. In order to calculate the equilibrium concentrations of these defects as functions of the thermodynamic variables of the system $BaTiO_{3-\delta}$, temperature (T), the activity of oxygen ($a_{O_2} \equiv Po_2/atm$) and the activity of a metallic component, say, BaO (a_{BaO}), at the atmospheric pressure, generally one has to consider the two external equilibria,[1]

$$O_O^\times = V_O^{\bullet\bullet} + 2e' + \frac{1}{2}O_2(g);$$

$$K_{Re} = [V_O^{\bullet\bullet}]n^2 a_{O_2}^{1/2} \tag{2.1}$$

$$BaO = Ba_{Ba}^\times + O_O^\times + V''''_{Ti} + 2V_O^{\bullet\bullet};$$

$$K_B = \frac{[V''''_{Ti}][V_O^{\bullet\bullet}]^2}{a_{BaO}} \tag{2.2}$$

and the two internal equilibria,

$$0 = e' + h^\bullet; \quad K_i = np \tag{2.3}$$

$$0 = V''_{Ba} + V''''_{Ti} + 3V_O^{\bullet\bullet}; \quad K_S = [V''_{Ba}][V''''_{Ti}][V_O^{\bullet\bullet}]^3 \tag{2.4}$$

along with the charge neutrality condition,

$$n + 2[V''_{Ba}] + 4[V''_{Ti}] + [A'_C] = p + 2[V_O^{\bullet\bullet}] \tag{2.5}$$

where [ ] denote the concentration of the irregular structure element therein ($n \equiv [e']$ and $p \equiv [h^\bullet]$). The mass-action law constant of the relevant reaction is denoted as $K_j (j = R, B, S, i)$ which may be represented as

$$K_j = K_j^o \exp\left(-\frac{\Delta H_j}{kT}\right) \tag{2.6}$$

where K_j^o is a pre-exponential factor and ΔH_j the enthalpy change of the relevant reaction j. In the present context, we assume that the acceptor type impurities (A'_C) are fixed-valent as it later turns out to be the case. (Otherwise, one has additionally to take into account the ionization equilibria of the acceptors themselves. [16, 19–21]).

Equation (2.5) indicates that there can be eight types of majority disorder, and obviously their configuration depends on the thermodynamic state of the system defined by the combination of T, a_{O_2} and a_{BaO}. There may be three possibilities of configuration: If the system is essentially pure or $[A'_C] \ll 2[V''_{Ba}] + 4[V''_{Ti}]$, one can neglect $[A'_C]$ in Eq. (2.5). Then, one may distinguish two possible configurations: (i) when ionic defects prevail or $K_S^{1/5} \gg K_i^{1/2}$ and (ii) when electronic defects prevail or $K_i^{1/2} \gg K_S^{1/5}$ in the stoichiometric regime ($\delta \approx 0$). Configuration for each case in the thermodynamic configuration space ($\log a_{O_2}$ vs. $\log a_{BaO}$) at a given temperature can be shown as in Fig. 1(a) and (b), respectively. [16, 22, 23] (iii) If the acceptor impurities, be they intentionally or unintentionally doped, are prevailing in the stoichiometric regime or $[A'_C] \gg 2[V''_{Ba}] + 4[V''_{Ti}]$, on the other hand, there can be only one configuration irrespective of whether $K_S^{1/5} \gg K_i^{1/2}$ or $K_i^{1/2} \gg K_S^{1/5}$. That is shown in Fig. 1(c).

Concentrations of all the ionic and electronic defects can be easily calculated as functions of a_{O_2} and a_{BaO} at a given temperature in each majority disorder regime in Fig. 1 by simultaneously solving Eqs. (2.1)–(2.5) simplified in terms of the majority type of disorder, but it is not completely pursued here. It is only pointed out that the slopes of boundaries between neighboring disorder regimes in Fig. 1 are as calculated [16, 22, 23] and "m" in each regime represents the oxygen exponent of the concentration of holes or electrons such that $p \propto a_{O_2}^{+m}$ and $n \propto a_{O_2}^{-m}$.

Up to now, there has appeared no experimental result for $BaTiO_3$ which may even hint a possibility of (e', $h^\bullet$), or $n \approx p$, being the majority disorder under any thermodynamic condition. All the conductivity results obtained from the "undoped" $BaTiO_3$ fit to the picture of either Fig. 1(a) or (c) as is seen shortly. We may, thus, conclude at the moment that the

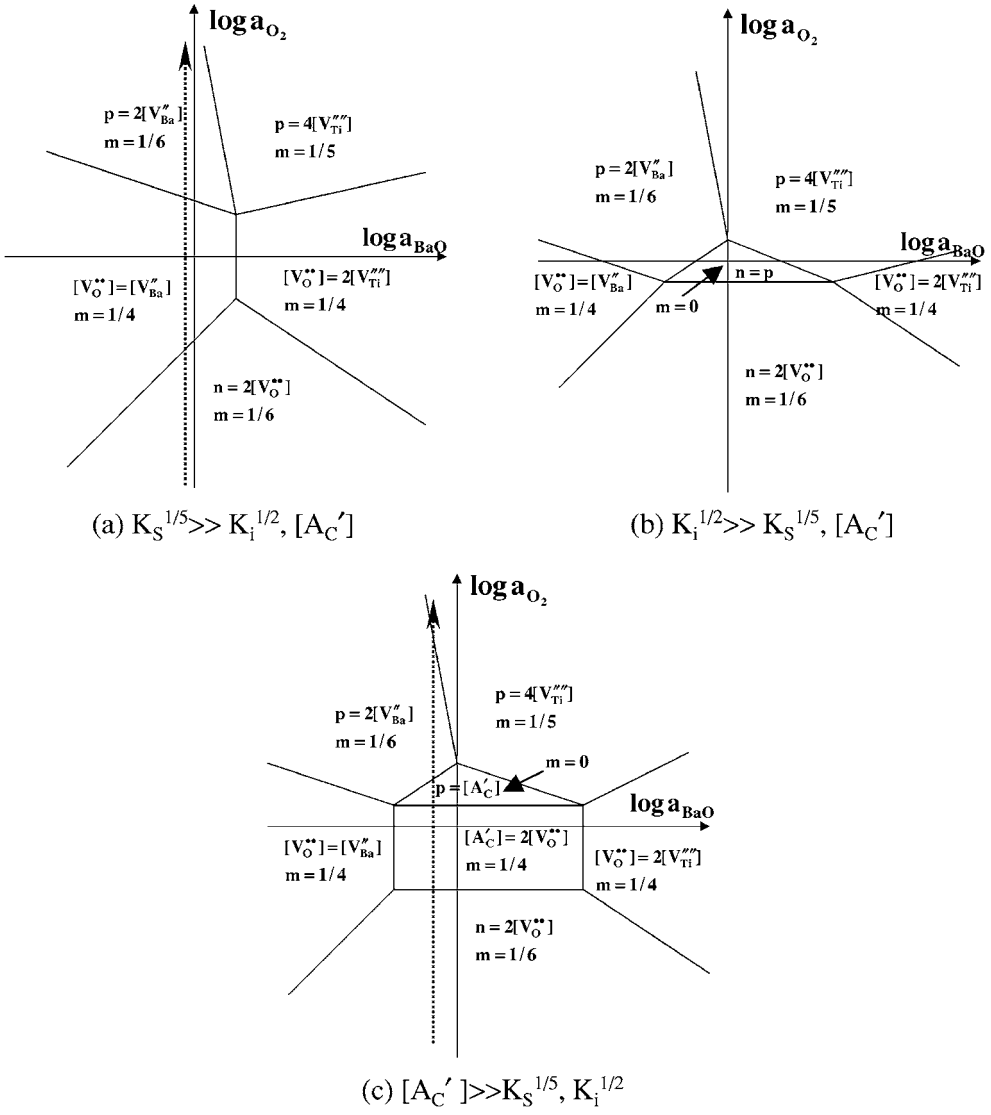

Fig. 1. Configuration of the majority types of disorder depending on the thermodynamic variables, a_{O_2} and a_{BaO} at a given temperature: (a) when $K_S^{1/5} \gg K_i^{1/2}$, $[A'_C]$ [16, 23]; (b) when $K_i^{1/2} \gg K_S^{1/5}$, $[A'_C]$ [22, 23]; (c) when $[A'_C] \gg K_S^{1/5}$, $K_i^{1/2}$ [16]. Here m denotes the oxygen partial pressure exponent of electron and hole densities such that $p \propto a_{O_2}^m$ and $n \propto a_{O_2}^{-m}$. The dotted lines in (a) and (c) represent the possible paths with increasing oxygen partial pressure in undoped $BaTiO_3$.

defect structure of "undoped" $BaTiO_3$ will be either of these.

It is noted that there are two ionic disorder regimes in Fig. 1(a): (V''_{Ba}, $V^{\bullet\bullet}_O$), ($V''_{Ti}{}''$, $V^{\bullet\bullet}_O$) or three in Fig. 1(c): (V''_{Ba}, $V^{\bullet\bullet}_O$), (A'_C, $V^{\bullet\bullet}_O$), ($V''_{Ti}{}''$, $V^{\bullet\bullet}_O$) in turn as a_{BaO} increases in the intermediate range[2] of a_{O_2} or between the exclusively n-type (i.e., lower a_{O_2}) and p-type (i.e., higher a_{O_2}) regimes. In all these regimes, the oxygen vacancy concentration is essentially fixed extrinsically (i.e., $[V^{\bullet\bullet}_O] \approx [A'_C]$) or intrinsically (i.e., $[V^{\bullet\bullet}_O] \approx [V''_{Ba}]$, $2[V''_{Ti}{}'']$) and hence, the concentrations of electrons and holes vary as $n \propto a_{O_2}^{-1/4}$ and $p \propto a_{O_2}^{+1/4}$ (i.e., $m = 1/4$) due to Eqs. (2.1) and (2.3). It, however, has, so far, not been unambiguously elucidated which of A'_C, V''_{Ba} and $V''_{Ti}{}''$ is really responsible for the a_{O_2}-region where the electronic conductivity varies as $\sigma_{el} \propto a_{O_2}^{\pm 1/4}$ [16, 17]. Furthermore, none of the exclusively p-type regimes, ($h^\bullet$, A'_C), ($h^\bullet$, V''_{Ba}) and ($h^\bullet$, $V''_{Ti}{}''$) has ever revealed

itself up to $a_{O_2} = 1$. For the simplicity sake, thus, we introduce the effective concentration of mono-valent acceptors [A′] such that

$$[A'] \equiv 2[V''_{Ba}] + 4[V''_{Ti}{}''] + [A'_C] \tag{2.7}$$

to rewrite Eq. (2.5) as

$$n + [A'] = p + 2[V^{\bullet\bullet}_O] \tag{2.8}$$

One can, then, simplify, without loss of generality, the configuration of Fig. 1(a) and (c), neglecting all the exclusively p-type regimes, only with two disorder regimes (e′, $V^{\bullet\bullet}_O$) and (A′, $V^{\bullet\bullet}_O$) as confirmed shortly by the electrical conductivity isotherms.

The defect concentrations of present interest in each of these disorder regimes are now calculated by solving Eqs. (2.1), (2.3), (2.4), and (2.8) as:

(i) In the disorder regime (e′, $V^{\bullet\bullet}_O$)

$$[V^{\bullet\bullet}_O] = \frac{n}{2} = \left(\frac{K_{Re}}{4}\right)^{1/3} a_{O_2}^{-1/6} \gg p \tag{2.9}$$

(ii) In the disorder regime (A′, $V^{\bullet\bullet}_O$)

$$[V^{\bullet\bullet}_O] = \frac{[A']}{2} \tag{2.10}$$

$$n = \sqrt{K_i}\left(\frac{a_{O_2}}{a^o_{O_2}}\right)^{-1/4} \tag{2.11}$$

$$p = \sqrt{K_i}\left(\frac{a_{O_2}}{a^o_{O_2}}\right)^{+1/4} \tag{2.12}$$

where $a^o_{O_2}$ is the oxygen activity at which $n = p = K_i^{1/2}$ or, due to Eq. (2.1),

$$a^o_{O_2} = \left(\frac{2K_{Re}}{[A']K_i}\right)^2 \tag{2.13}$$

The defect concentrations are varying against oxygen activity e.g. at 1000°C as illustrated in Fig. 2.

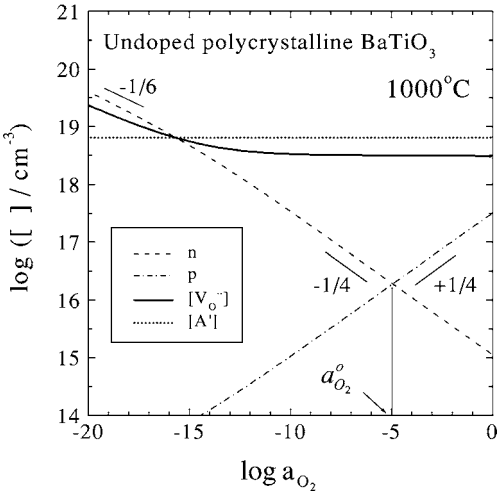

Fig. 2. Defect concentrations vs. oxygen activity of "undoped" $BaTiO_3$ at 1000°C. For the calculation the following values were used: $K_i = 3.6 \times 10^{32}$ cm^{-6} (from Eq. (4.9)), $K_{Re} = 3.9 \times 10^{48}$ cm^{-9} (from Eq. (4.13)) and $[A'] = 6.4 \times 10^{18}$cm^{-3} (from Eq. (4.12) in the text).

3. Electrical Conductivity

3.1. Compilation of Data

As mentioned earlier, the d.c. electrical conductivity among others has been the most extensively documented mainly for the purpose of elucidation of the defect structure. The conductivity data at 800°, 900°, 1000°, and 1100°C that were reported previously, [16, 24–31] are all compiled in Fig. 3. It is seen that the conductivity apparently varies as $a_{O_2}^{-1/6}$, $a_{O_2}^{-1/4}$ and $a_{O_2}^{+1/4}$ in turn as a_{O_2} increases, complying with the shift of majority disorder types from (n, $V^{\bullet\bullet}_O$) to ($V^{\bullet\bullet}_O$, A′) according to Figs. 1 or 2. This trend of variation is exactly reproduced by the authors [9, 14] as shown in Fig. 4 not only for the "undoped" (a), but also for the acceptor(Al)-doped single crystal (b). Upon comparison, it is seen that the trend of conductivity variation of the "undoped" is quite similar to that of the acceptor-doped. This fact supports that if there are any background impurities as majority disorder in the "undoped", they will be of acceptor-type [32]. Nevertheless, while for the latter clearly $A' = Al'_{Ti}$, but for the "undoped", the effective acceptor A′ still remains unidentified: One cannot tell whether $A' = V''_{Ba}$ or $V''_{Ti}{}''$ or A'_C, see Eq. (2.7).

3.2. Correlation with Defect Structure

It is reported that the self-diffusion coefficients of O and Ba are 4.58×10^{-12} cm^2 sec^{-1} and 5.28×10^{-16} cm^2 sec^{-1}, respectively, e.g., at 1000°C (See Section 4), and that the migration enthalpy of Ti ions is about 5 times larger than that of Ba ions [18]. We may, thus, safely assume that at normal temperatures, the cations, Ba^{2+}

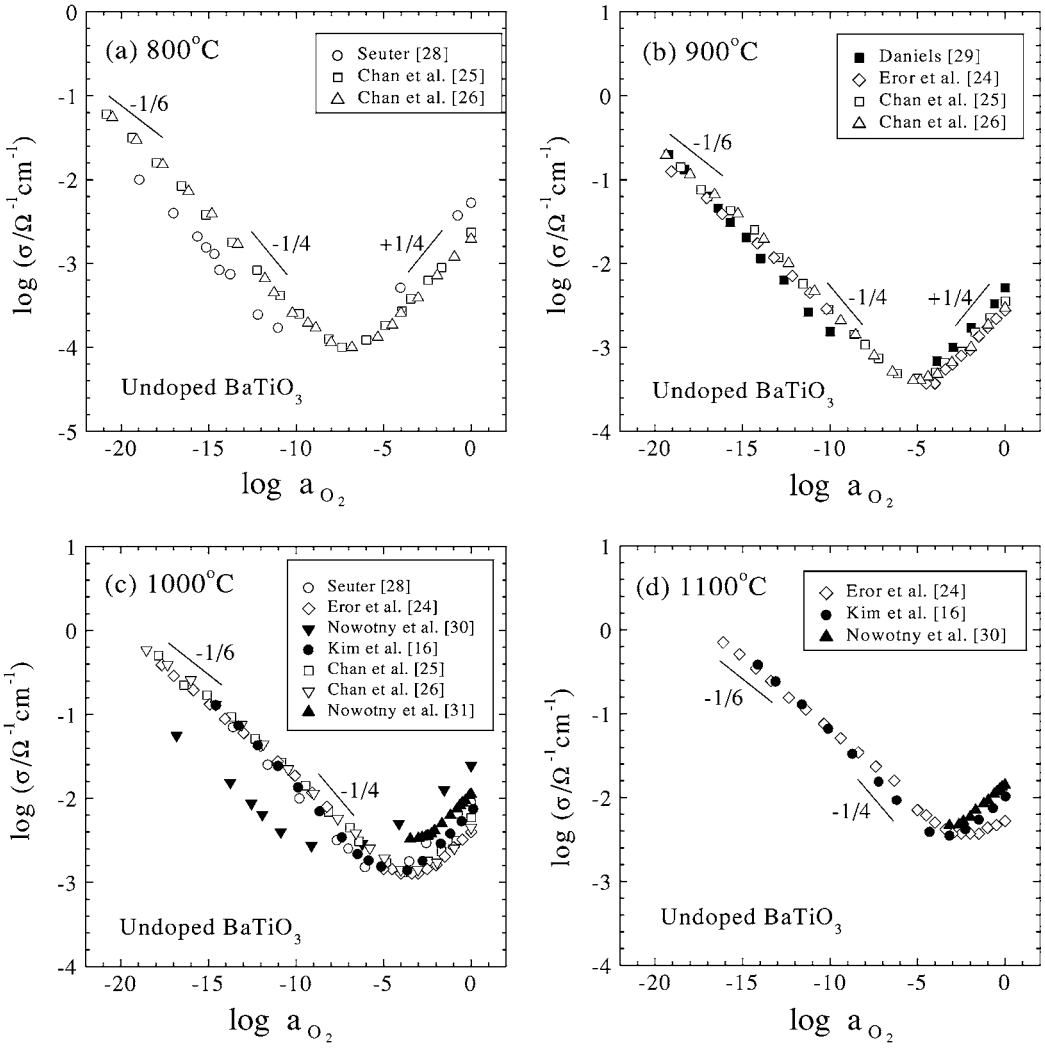

Fig. 3. Electrical conductivity isotherms reported thus far on undoped $BaTiO_3$ at (a) 800°, (b) 900°, (c) 1000° and (d) 1100°C.

and Ti^{4+}, be practically immobile compared with the oxide ions. We may, thus, take only oxide anions O^{2-} and electrons e^- as the mobile, charged components or equivalently, $V_O^{\bullet\bullet}$, e' and $h^\bullet$ in terms of defects. We further assume that the electrochemical mobility of each type of carrier, u_k, is independent of defect concentrations at given temperature.

When there are both electrons and holes as electronic charge carriers, the electronic conductivity, σ_{el}, can be written in general as [33, 34]

$$\sigma_{el} = \sigma_n + \sigma_p = \sigma_{el,m}\cosh\left(\frac{1}{2}\ln\alpha\right) \tag{3.1}$$

where

$$\alpha \equiv \frac{\sigma_p}{\sigma_n} = \frac{p}{nb}; \quad b \equiv \frac{u_n}{u_p} \tag{3.2}$$

and $\sigma_{el,m}$ denotes the minimum of σ_{el} where $\sigma_n = \sigma_p = \sigma_{el,m}/2$, or

$$\sigma_{el,m} \equiv 2e\sqrt{K_i}\sqrt{u_u u_p} \tag{3.3}$$

It is noted that Eq. (3.1) works for any semiconductor inasmuch as Eq. (2.3) is valid. If $\alpha \gg 1$ or $\sigma_p \gg \sigma_n$, then Eq. (3.1) obviously reduces to $\sigma_{el} \approx peu_p = \sigma_p$ and vice versa to $\sigma_{el} \approx neu_n = \sigma_n$.

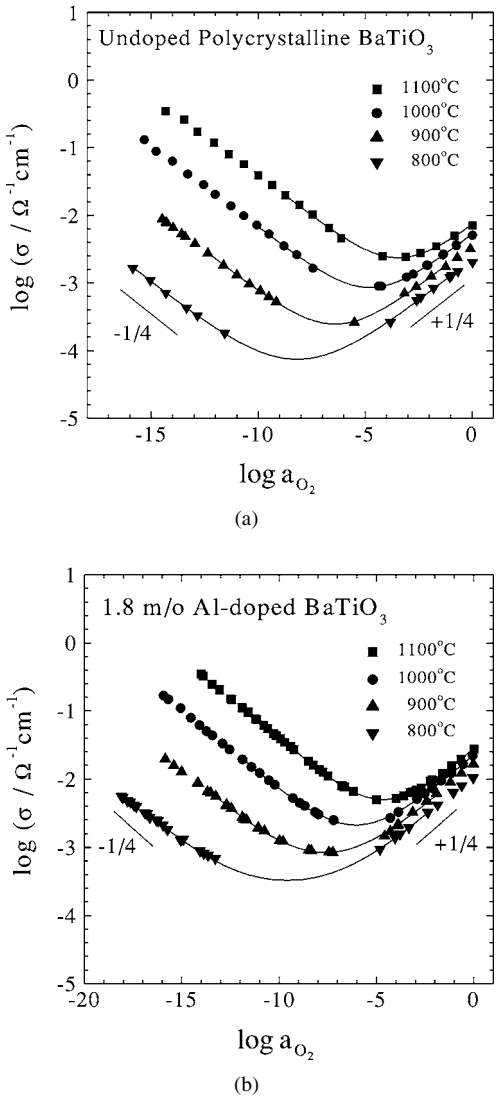

Fig. 4. Electrical conductivity isotherms of (a) "undoped" polycrystalline and (b) 1.8 m/o Al-doped single crystal $BaTiO_3$ at different temperatures, respectively. The solid lines are the best-fitted results to Eq. (3.8) in the text.

The partial ionic conductivity is written due to Nernst-Einstein equation as

$$\sigma_{\text{ion}} = \frac{4e^2[\text{O}_\text{O}^\times]D_\text{O}}{kT} = \frac{4e^2[\text{V}_\text{O}^{\bullet\bullet}]D_{\text{V}_\text{O}}}{kT} \tag{3.4}$$

The total conductivity $\sigma(=\sigma_{\text{el}} + \sigma_{\text{ion}})$ of our system is now evaluated specifically in each disorder regime in Fig. 2 as follows:

(i) In the disorder regime (e', $\text{V}_\text{O}^{\bullet\bullet}$):

Because $n \gg p$ and $u_n \gg u_{\text{V}_\text{O}}$, the total conductivity is essentially the same as the conductivity of electrons or, due to Eq. (2.9),

$$\sigma \approx \sigma_n = eu_n(2K_{\text{Re}})^{1/3}a_{\text{O}_2}^{-1/6} \tag{3.5}$$

(ii) In the disorder regime (A', $\text{V}_\text{O}^{\bullet\bullet}$):

The partial conductivities of electrons and holes may be represented, due to Eqs. (2.11) and (2.12), as

$$\sigma_n = \frac{\sigma_{\text{el},m}}{2}\left(\frac{a_{\text{O}_2}}{a^*_{\text{O}_2}}\right)^{-1/4} \quad ; \quad \sigma_p = \frac{\sigma_{\text{el},m}}{2}\left(\frac{a_{\text{O}_2}}{a^*_{\text{O}_2}}\right)^{+1/4} \tag{3.6}$$

Here, $a^*_{\text{O}_2}$ is the oxygen activity at which $\sigma_{\text{el}} = \sigma_{\text{el},m}$ or $\sigma_n = \sigma_p = \sigma_{\text{el},m}/2$, and is, thus, related to the oxygen activity $a^o_{\text{O}_2}$, where $n = p$ or Eq. (2.13), again due to Eqs. (2.11) and (2.12), as

$$a^*_{\text{O}_2} = b^2 a^o_{\text{O}_2} \tag{3.7}$$

The partial ionic conductivity, on the other hand, may be regarded as being independent of oxygen partial pressure because $[\text{V}_\text{O}^{\bullet\bullet}]$ is essentially fixed by the effective acceptors $[A']$ at given temperature, see Fig. 2. The total electrical conductivity is finally represented as

$$\sigma = \sigma_{\text{el},m}\cosh\left[\frac{1}{4}\ln\left(\frac{a_{\text{O}_2}}{a^*_{\text{O}_2}}\right)\right] + \sigma_{\text{ion}} \tag{3.8}$$

One can recognize upon comparison with Eq. (3.1) that $\alpha = (a_{\text{O}_2}/a^*_{\text{O}_2})^{1/2}$ in this specific disorder regime.

3.3. *Defect-Chemical Analysis*

The isotherms in Fig. 4 are nonlinear-least-squares (NLLS) fitted to Eq. (3.8) only in the neighborhood of the conductivity minima. The results are as depicted by the solid lines in Fig. 4. As is seen, the conductivity isotherms are quite precisely described by Eq. (3.8) with the fitting parameters, $\sigma_{\text{el},m}$, σ_{ion} and $a^*_{\text{O}_2}$ evaluated as listed in Table 1. As we now know the values for $\sigma_{\text{el}}(=\sigma - \sigma_{\text{ion}})$ and $\sigma_{\text{el},m}$, we can calculate, by using Eq. (3.1) the conductivity ratio, α in Eq. (3.2) upon each isotherm over the entire range of oxygen partial

Table 1. Parameters, $\sigma_{el,m}$, σ_{ion} and $a^*_{O_2}$ as evaluated from the isotherms of total electrical conductivity of the "undoped" $BaTiO_3$.

T/K	$\log(\sigma_{el,m}/\Omega^{-1}\,cm^{-1})$	$\log(\sigma_{ion}/\Omega^{-1}\,cm^{-1})$	$\log a^*_{O_2}(=P^*_{O_2}/atm)$
1073	$-(4.401 \pm 0.008)$	$-(4.463 \pm 0.089)$	$-(8.174 \pm 0.020)$
1173	$-(3.756 \pm 0.008)$	$-(4.155 \pm 0.065)$	$-(6.400 \pm 0.020)$
1273	$-(3.191 \pm 0.010)$	$-(3.681 \pm 0.083)$	$-(4.772 \pm 0.025)$
1373	$-(2.740 \pm 0.015)$	$-(3.272 \pm 0.100)$	$-(3.447 \pm 0.041)$

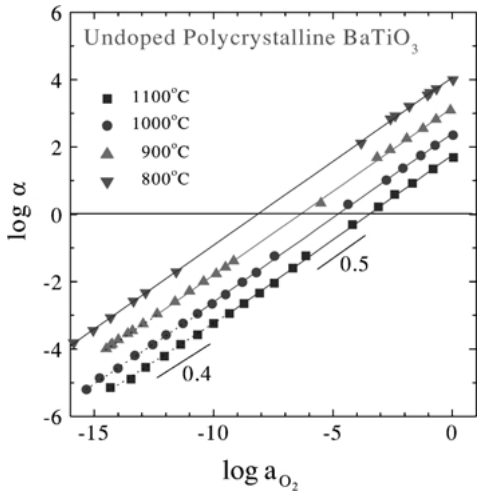

Fig. 5. The conductivity ratio, $\log \alpha$ vs. $\log a_{O_2}$ for undoped $BaTiO_3$. The solid lines with an ideal slope of $2m = 0.5$ represent the regions of the majority disorder (A', $V_O^{\bullet\bullet}\cdot$) at different temperatures, and the dotted lines with a smaller slope indicate the shift of the majority disorders to (e', $V_O^{\bullet\bullet}$). See Eq. (3.9) in the text.

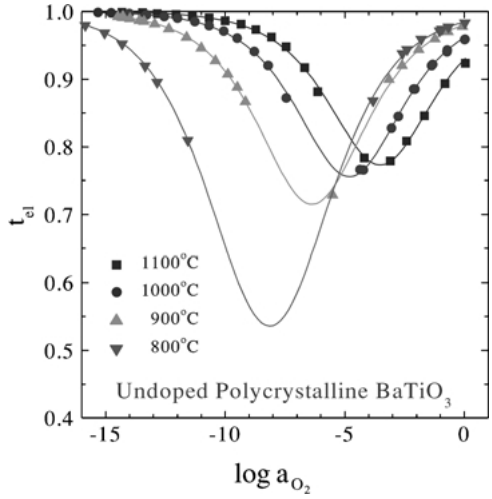

Fig. 6. Electronic transference number of the "undoped" $BaTiO_3$ vs. oxygen activity at different temperatures. The solid lines are the best-fitted to Eq. (3.10) in the text.

pressure examined in Fig. 4. The results are as shown in Fig. 5.

As $\sigma_p \propto a_{O_2}^{+m}$ and $\sigma_n \propto a_{O_2}^{-m}$ as long as Eq. (2.3) remains valid, one has

$$\left(\frac{\partial \log \alpha}{\partial \log a_{O_2}}\right)_T = 2m \tag{3.9}$$

It is seen in Fig. 5 that over an extended range of $\log a_{O_2}$ around each conductivity minimum ($\log \alpha = 0$), $2m = 0.5$, but becomes smaller as a_{O_2} further goes lower, e.g., $2m = 0.4$ at 1100°C. This trend, however, turns less conspicuous, the lower the temperature, so that $2m = 0.5$ over the entire a_{O_2} range at 800°C. This is exactly in accord with the defect structure in Fig. 2, thus supporting its validity.

One may use these values for α to evaluate the electronic transference number, t_{el}, as

$$t_{el} = \frac{\sigma_{el,m}}{\sigma} \cosh\left(\frac{1}{2}\ln \alpha\right) \tag{3.10}$$

The results are illustrated in Fig. 6, where the solid lines are the best-fitted by using $\alpha = \alpha(a_{O_2})$ in Fig. 5.

Figure 7 shows the variation of $\sigma_{el,m}$ and σ_{ion}, as extracted from Fig. 4, against reciprocal temperature. It is noted that the experimental value for $\sigma_{ion}(=3.4\times 10^{-5}\ \Omega^{-1}cm^{-1})$ at 800°C is appreciably off the extrapolated ($1.9 \times 10^{-5}\ \Omega^{-1}cm^{-1}$) from the main trend of variation at the higher temperatures, while the variation of $\sigma_{el,m}$ remains consistent in the entire temperature range. Possible reasons for this deviation will be briefly mentioned in the following section. Rejecting the datum at 800°C, thus, the ionic conductivity may be best estimated as

$$\sigma_{ion}/Scm^{-1} = \frac{(2.77 \pm 0.16) \times 10^5}{T} \times \exp\left(-\frac{1.520 \pm 0.006\ eV}{kT}\right) \tag{3.11}$$

and plotted against reciprocal temperature in Fig. 7. It is noted in Fig. 6 that the minimum electronic

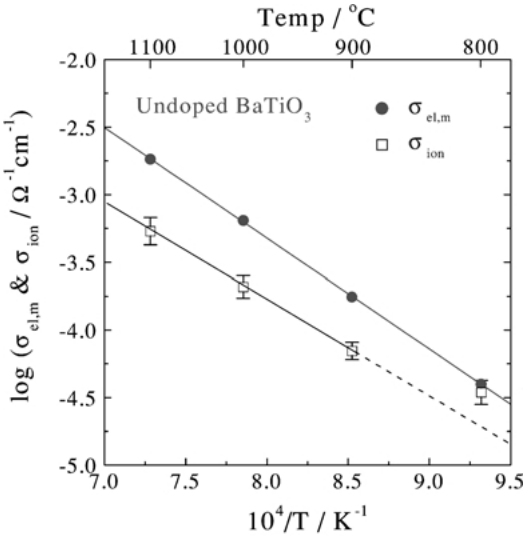

Fig. 7. Variation of $\sigma_{el,m}$ and σ_{ion}, as extracted from Fig. 4 vs. reciprocal temperature. Note that while $\sigma_{el,m}$ remains consistent over the entire temperature range, σ_{ion} at 800°C is appreciably off the main trend.

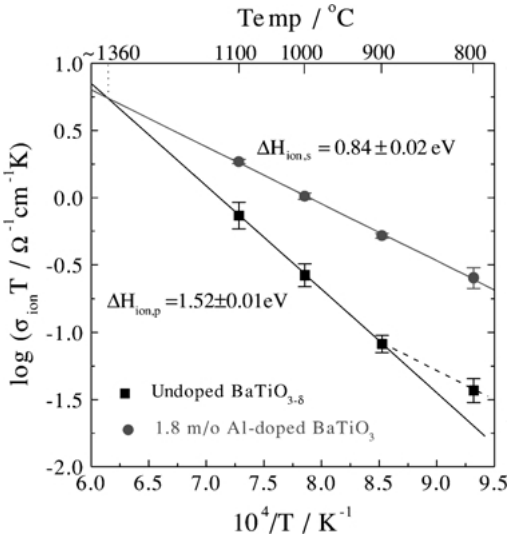

Fig. 8. $\log(\sigma_{ion}T)$ vs. reciprocal temperature. $\Delta H_{ion,p}$ and $\Delta H_{ion,s}$ denote the activation enthalpies of $\sigma_{ion}T$ for the polycrystalline, "undoped" $BaTiO_3$ and 1.8 m/o Al-doped single crystal $BaTiO_3$, respectively.

transference number at 800°C appears to be markedly smaller than what is expected from the values at the higher temperatures. This is attributed to the ionic conductivity at 800°C being appreciably larger than the extrapolated from the trend of variation at the higher temperatures. For the Al-doped single crystal, however, this sort of thing does not appear and the ionic conductivity is represented just by a single line over the entire temperature range or

$$\sigma_{ion}/\mathrm{Scm}^{-1} = \frac{(2.25 \pm 0.08) \times 10^3}{T} \times \exp\left(-\frac{0.84 \pm 0.02\ \mathrm{eV}}{kT}\right) \qquad (3.12)$$

as shown in Fig. 8.

In passing, it is emphasized that one can only get $\sigma_n, \sigma_p, \sigma_{el,m}$, σ_{ion}, and $a^*_{O_2}$ from the total conductivity isotherms in the electrons/holes/ions mixed regime. No further analysis is possible beyond this point because we are lacking in the information on carrier mobilities or concentrations. These information can only be made available by another property measurement of either chemical diffusivity or nonstoichiomety.

4. Chemical Diffusivity

4.1. Compilation of Data

Very limited number of chemical diffusion data have been reported up to date on $BaTiO_3$ whether doped or not. Wernicke [35] measured the chemical diffusivity of polycrystalline, undoped and La-doped $BaTiO_3$ in an oxygen partial pressure range, $0.1 \le a_{O_2} \le 1$, at temperatures, $1023 \le T/K \le 1273$ and $1223 \le T/K \le 1373$, respectively, by a conductivity relaxation technique. Maier et al. [36] reported on the chemical diffusivities of both polycrystalline and single crystal $BaTiO_3$ in air atmosphere at temperatures, $873 \le T/K \le 933$, as determined by a polarization technique in electron-blocking cells. Recently, Müller and Härdtl [37] have determined the chemical diffusivity of both polycrystalline and single crystal $BaTiO_3$ in an oxygen partial pressure range, $0.1 \le a_{O_2} \le 0.2$, at temperatures in the range of $973 \le T/K \le 1473$, via the conductivity relaxation technique. Nowotny and Rekas [38] also reported the chemical diffusivity on Nb-doped $BaTiO_3$ in the temperature range of $1150 \le T/K \le 1425$ at 0.002 atm oxygen partial pressure. In addition, Shirasaki et al. [39, 40] measured the oxygen tracer diffusivity on polycrystalline $BaTiO_3$ in an oxygen partial pressure, $a_{O_2} = 0.05$, as a function of temperature in the range of $1043 \le T/K \le 1703$ by using an O^{18}/O^{16}

Table 2. Experimental conditions of diffusivity measurements on $BaTiO_3$ in Fig. 9.

No.	Author(s)	D	Range	Measurement	System	Ref.
1	Müller and Härdtl	$\tilde{D}$	$973 \le T/K \le 1473$ $a_{O_2} = 0.1$	Conductivity relaxation	Single crystal undoped $BaTiO_3$	[37]
2	Müller and Härdtl	$\tilde{D}$	$973 \le T/K \le 1473$ $a_{O_2} = 0.1$	Conductivity relaxation	Polycrystalline undoped $BaTiO_3$	[37]
3	Wernicke	$\tilde{D}$	$1023 \le T/K \le 1273$ $a_{O_2} = 0.1$	Conductivity relaxation	Polycrystalline undoped $BaTiO_3$	[35]
4	Maier et al.	$\tilde{D}$	$873 \le T/K \le 923$ $a_{O_2} = 0.21$	Polarization cell technique	Polycrystalline undoped $BaTiO_3$	[36]
5	Maier et al.	$\tilde{D}$	$903 \le T/K \le 933$ $a_{O_2} = 0.21$	Polarization cell technique	Single crystal undoped $BaTiO_3$	[36]
6	Shirasaki et al.	D^*_O	$770 \le T/K \le 1430$ $a_{O_2} = 0.05$	^{18}O exchange technique	Polycrystalline undoped $BaTiO_3$	[39]
7	Shirasaki et al.	D^*_O	$1040 \le T/K \le 1703$ $a_{O_2} = 0.05$	^{18}O exchange technique	Polycrystalline 10m/o La-doped $BaTiO_3$	[39]
8	Shirasaki et al.	D^*_O	$1190 \le T/K \le 1520$ $a_{O_2} = 0.07$	^{18}O exchange technique	Polycrystalline 0.01m/o La-doped $BaTiO_3$	[40]
9	Wernicke	$\tilde{D}$	$1223 \le T/K \le 1373$ $a_{O_2} = 0.1$	Conductivity relaxation	Polycrystalline 0.5m/o La-doped $BaTiO_3$	[35]
10	Nowotny and Rekas	$\tilde{D}$	$1150 \le T/K \le 1425$ $a_{O_2} = 0.002$	Conductivity relaxation	Polycrystalline 0.05m/o Nb-doped $BaTiO_3$	[38]
11	Garcia-Verduch and Lindner	D^*_{Ba}	$1157 \le T/K \le 1453$	Tracer diffusion	Polycrystalline $BaTiO_3$	[41]

gas-exchange technique. Regarding cation self-diffusion, only one set of data has been reported on Ba-tracer diffusion by Garcia-Verduch and Lindner [41]. All these are summarized in Table 2 and compared with each other in Fig. 9. As is seen, the chemical diffusivity of $BaTiO_3$ has so far been measured only in a limited range of oxygen partial pressure, $a_{O_2} \ge 0.1$, where $BaTiO_3$ is essentially of p-type if "undoped", see Fig. 2.

Recently, the authors [9, 14] have determined by a conductivity relaxation technique the chemical diffusion coefficient of the "undoped" and 1.8 m/o Al-doped $BaTiO_3$, respectively, against oxygen partial pressure in the widest ever range of oxygen partial pressure, $10^{-16} \le a_{O_2} \le 1$ at temperatures of 800°, 900°, 1000°, and 1100°C, respectively. The results, $\tilde{D}$ vs. log a_{O_2}, are shown in Fig. 10(a) and (b), respectively. The specimens employed are the same as those on which the electrical conductivities, Fig. 4(a) and (b), have been measured, respectively. Upon comparison of the chemical diffusivity with the corresponding conductivity, one can see that, over the n- to p-type transition region of a_{O_2} across the conductivity minimum, the chemical diffusivity varies convex-upwardly leaving a maximum approximately at the oxygen activity $a^*_{O_2}$ where the conductivity minimum falls. This trend of variation is more clearly seen for the 1.8 m/o Al-doped system in Fig. 10(b). This sort of behavior of chemical diffusivity has earlier been reported only on the systems of α-$Ag_{2+\delta}S$ [42] and α'-$Ag_{2+\delta}Te$ [43]. For the systems of oxides, however, this makes the very first observation of the kind.

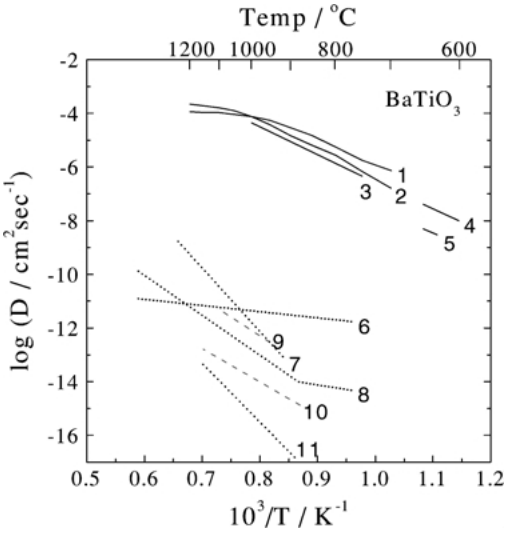

Fig. 9. Compilation of diffusivities reported thus far on $BaTiO_3$. Solid lines (1–5): chemical diffusivity for the undoped; Dashed lines (9, 10): chemical diffusivity for the donor(La)-doped; Dotted lines (6–8): oxygen tracer diffusivity; Dotted line (11): tracer diffusivity of Ba. See Table 2 for details of the data.

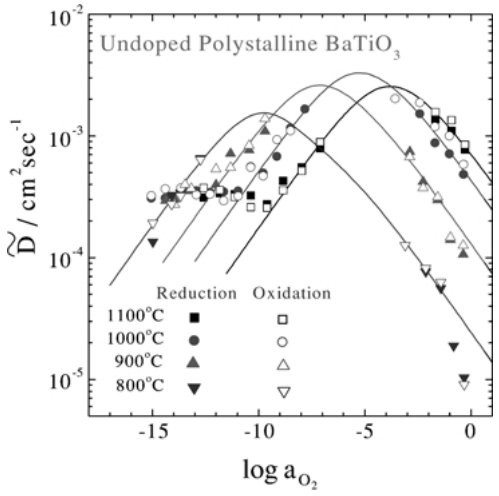

(a)

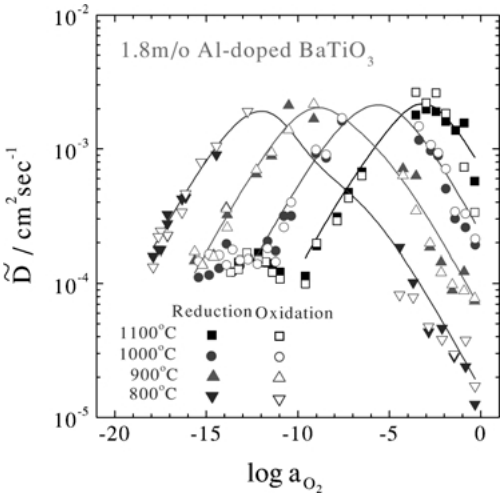

(b)

Fig. 10. Chemical diffusivity of (a) undoped and (b) 1.8 m/o Al-doped $BaTiO_3$, respectively, vs. oxygen activity at different temperatures. The solid lines are the best-fitted to Eq. (4.7) in the text.

The authors' own results that correspond to air atmosphere are compared with the literature data (that are all for $\log a_{O_2} > -0.1$) in detail in Fig. 11. They are in reasonable agreement with the reported in trend against temperature and magnitude, however, mark the largest at 1000° and 1100°C. It seems to be quite consistent that the trend of variation of $\tilde{D}$ vs. $1/T$ deviates (elbow-upwardly) from linearity around 1000°C and higher. (This deviation is attributed to change of the thermodynamic factor and electronic transference

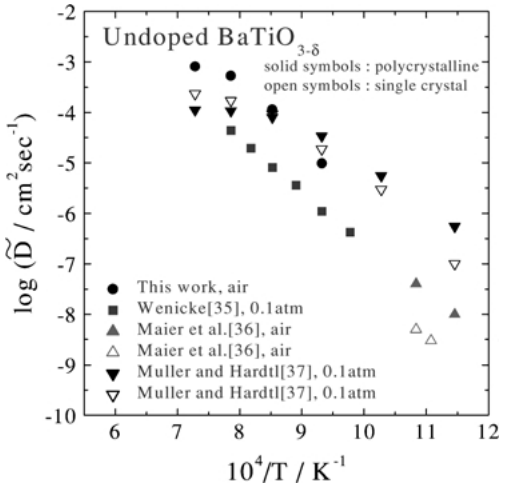

Fig. 11. Detailed comparison of the authors' own results for the air atmosphere with all the reported values on the chemical diffusivity of undoped $BaTiO_3$. For the experimental details of the other authors, see Table 2.

number with temperature in the fixed atmosphere, air, see below.) The present results in the temperature range of $T \leq 1273$ K may be best estimated, for the purpose of comparison, as

$$\tilde{D}/\mathrm{cm}^2\,\mathrm{sec}^{-1} = (1.38 \pm 0.34) \times 10^6 \times \exp\left(-\frac{2.37 \pm 0.21\ \mathrm{eV}}{kT}\right) \qquad (4.1)$$

The activation energies reported are 2.09 eV [35] and 2.70 eV [37], which are all comparable with the present value, 2.37 eV.

4.2. *Correlation with Defect Structure*

When practically only oxide ions and electrons are mobile in ternary $BaTiO_{3-\delta}$,[3] the chemical diffusivity may be written in accord with Wagner [44] as

$$\tilde{D} = -\frac{D_{V_O} t_{el}}{2}\left(\frac{\partial \ln[V_O^{\bullet\bullet}]}{\partial \ln a_{O_2}}\right)^{-1} \qquad (4.2)$$

or, due to the Nernst-Einstein equation, Eq. (3.4),

$$\tilde{D} = -\frac{kT\sigma_{ion} t_{el}}{8e^2}\left(\frac{\partial [V_O^{\bullet\bullet}]}{\partial \ln a_{O_2}}\right)^{-1} \qquad (4.2a)$$

The term within the parentheses on the right hand side is conventionally called a thermodynamic factor. In order to evaluate the chemical diffusivity, one has first to identify t_{el} and the thermodynamic factor against oxygen partial pressure. The former has already been evaluated from the conductivity measurement in Fig. 6. The latter is now identified in each disorder regime of Fig. 2 below.

(i) In the disorder regime (e', $V_O^{\bullet\bullet}$):

Eq. (2.8) yields the thermodynamic factor as

$$\frac{\partial \ln[V_O^{\bullet\bullet}]}{\partial \ln a_{O_2}} = -\frac{1}{6} \tag{4.3}$$

and $t_{el} \approx 1$ due to Eq. (2.13). Equation (4.2) thus takes a very familiar form

$$\tilde{D} \approx 3D_{V_O} \tag{4.4}$$

(ii) In the disorder regime (A', $V_O^{\bullet\bullet}$):

By substituting Eqs. (2.11) and (2.12) into Eq. (2.8), one obtains,

$$\begin{aligned}[V_O^{\bullet\bullet}] &= \frac{[A']}{2} + \frac{1}{2}(n-p) \\ &= \frac{[A']}{2} - \sqrt{K_i}\sinh\left(\frac{1}{4}\ln\frac{a_{O_2}}{a_{O_2}^o}\right)\end{aligned} \tag{4.5}$$

Thus, the thermodynamic factor takes the form

$$\left(\frac{\partial \ln[V_O^{\bullet\bullet}]}{\partial \ln a_{O_2}}\right)^{-1} \approx -\frac{2[A']}{\sqrt{K_i}\cosh\left(\frac{1}{4}\ln\frac{a_{O_2}}{a_{O_2}^o}\right)} \tag{4.6}$$

as $[A'] \gg n - p$. Even if $[V_O^{\bullet\bullet}]$ is practically fixed by the effective acceptors or $[V_O^{\bullet\bullet}] \approx [A']/2$ in this a_{O_2} region, its a_{O_2}-dependence is given as that of the difference between the minority carrier concentrations, $n - p$.

Accordingly, Eqs. (4.2) or (4.2a) is rewritten as

$$\tilde{D} = \frac{\tilde{D}^o t_{el}}{\cosh\left(\frac{1}{4}\ln\frac{a_{O_2}}{a_{O_2}^o}\right)} \tag{4.7}$$

where

$$\tilde{D}^o = \frac{kT\sigma_{ion}}{2e^2\sqrt{K_i}} \tag{4.8}$$

4.3. Defect-Chemical Analysis

Upon comparison with the variation of the conductivity isotherms in Figs. 4(a) or 5, the diffusivity data in the regions of $\log a_{O_2} < -13$, -11 and -10 at 900°, 1000°, and 1100°C, respectively, in Fig. 10(a) may be regarded as being in transition towards the defect regime of (e', $V_O^{\bullet\bullet}$). They, thus, cannot be fitted to Eq. (4.7). In addition, the two data in $\log a_{O_2} > -1$ at 800°C in particular appear also to be far off the expected values from the major trend of variation. It may be attributed to the trapping effect by acceptor-type disorders (i.e., A' being no longer fixed-valent), [21, 45, 46] or to the majority type of disorder already being in transition to another regime, say, ($h^{\bullet}$, A') [i.e., no longer in the regime of (A', $V_O^{\bullet\bullet}$)]. The exact reason is not immediately clear. Those data are thus precluded, and the rest of the data that obviously belong to the electrons/holes/ions mixed regime (A', $V_O^{\bullet\bullet}$) are the best fitted to Eq. (4.7) with the use of the electronic transference number in Fig. 6. The results are as depicted by the solid lines in Fig. 10(a) for the "undoped" and the fitting parameters, $\tilde{D}^o$ and $a_{O_2}^o$, are listed in Table 3. Similarly, the solid lines in Fig. 10(b) for the Al-doped are also the best fitted to Eq. (4.7) [14]. As is seen, Wagner's classic theory explains quite satisfactorily the variation of $\tilde{D}$ for both cases. Clearly, the presence of a maximum on a chemical diffusivity isotherm is attributed to the fact that the thermodynamic factor becomes maximum at $a_{O_2}^o$ or the electronic stoichiometric composition ($n = p$).

From the total conductivity isotherms in Fig. 4, we have deconvoluted $\sigma_n, \sigma_p, \sigma_{el,m}$ (Eq. (3.3)), σ_{ion} (Eq. (3.4)) and $a_{O_2}^*$ (Eq. (3.7)). From the chemical

Table 3. Parameters, $\tilde{D}^o$ and $a_{O_2}^o$, as evaluated from the isotherms of chemical diffusivity for the undoped $BaTiO_3$.

T/K	$\log(\tilde{D}^o/\text{ cm}^2\text{ s}^{-1})$	$\log a_{O_2}^o$
1073	$-(2.590 \pm 0.038)$	$-(9.269 \pm 0.151)$
1173	$-(2.446 \pm 0.019)$	$-(6.934 \pm 0.080)$
1273	$-(2.364 \pm 0.016)$	$-(5.140 \pm 0.072)$
1373	$-(2.484 \pm 0.015)$	$-(3.725 \pm 0.066)$

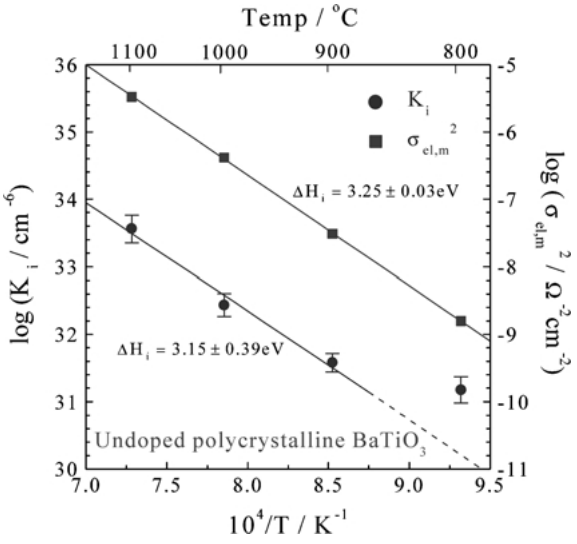

Fig. 12. Log K_i and log $\sigma^2_{\mathrm{el},m}$ vs. reciprocal temperature. The solid lines are the best-fitted with the datum at 800°C rejected for K_i.

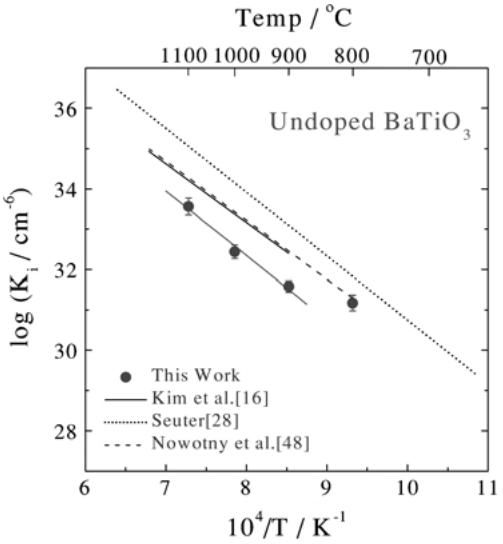

Fig. 13. Comparison of all the reported values of K_i (Table 4 in the text).

diffusivity isotherms in Fig. 10, the information on $\tilde{D}^o$ (Eq. (4.8)) and $a^o_{\mathrm{O}_2}$ (Eq. (2.13)). By combining these pieces of information, one can evaluate the defect parameters without using any ad hoc assumptions regarding, e.g., the densities of states and carrier mobilities, contrary to the previous works [16, 24, 26, 28–32, 47, 48].

4.3.1. Intrinsic Electronic Equilibrium Constant. The intrinsic electronic equilibrium constant K_i of Eq. (2.3) is evaluated from Eq. (4.8) by using the numerical values for σ_{ion} and $\tilde{D}^o$ in Tables 1 and 3, respectively. The result is as shown in Fig. 12. As is seen, the value for K_i at 800°C is again markedly off the main trend of variation. The rest in the temperature range of $1173 \leq T/K \leq 1373$ are the best estimated as

$$K_i/\mathrm{cm}^{-6} = \left(1.06^{+36.8}_{-1.03}\right) \times 10^{45} \exp\left(-\frac{3.15 \pm 0.39\ \mathrm{eV}}{kT}\right) \qquad (4.9)$$

Up to now, this constant has been evaluated by assuming in a way or the other the values for the density of states and/or the carrier mobilities [16, 28, 29, 48]. All the literature values thereby are compiled in Table 4 and compared in Fig. 13. Nevertheless, the literature values for K_i are favorably compared with the present one.

The band gap has often been estimated from $\sigma_{\mathrm{el},m}$ on the basis of Eq. (3.3) with temperature dependence of the carrier mobilities ignored [16, 24, 26–30, 48]. For comparison, $\sigma^2_{\mathrm{el},m}$ is co-plotted in Fig. 12. An activation enthalpy for $\sigma_{\mathrm{el},m}$, 3.25 ± 0.03 eV is quite close to the thermal band gap, $\Delta H_i = 3.15$ eV, in Eq. (4.9). In view of Eq. (3.3), this fact implies that the product of mobilities, $u_n u_p$ is insensitive to temperature as will be confirmed shortly.

4.3.2. Mobilities of Electronic Carriers. One can get the mobility product, $u_n u_p$, from the minimum electronic conductivity, Eq. (3.3), in association with K_i

Table 4. Comparison of K_i values reported on undoped $BaTiO_3$.

Author(s)	K_i/cm^{-6}	Measurement	Ref.
Song and Yoo	$1.06 \times 10^{45} \exp(-\frac{3.15\,\mathrm{eV}}{kT})$	Conductivity, chemical diffusivity	[10]
Kim et al.	$6.80 \times 10^{44} \exp(-\frac{2.90\,\mathrm{eV}}{kT})$	Conductivity, thermoelectric power	[16]
Seuter	$3.96 \times 10^{46} \exp(-\frac{3.15\,\mathrm{eV}}{kT})$	Conductivity, thermoelectric power	[28]
Nowotny and Rekas	$8.55 \times 10^{44} \exp(-\frac{2.91\,\mathrm{eV}}{kT})$	Conductivity, thermoelectric power	[48]

Table 5. Numerical values for mobilities of electrons and holes.

T/K	$u_n/\mathrm{cm}^2\ \mathrm{V}^{-1}\ \mathrm{sec}^{-1}$	$u_p/\mathrm{cm}^2\ \mathrm{V}^{-1}\ \mathrm{sec}^{-1}$
1073	0.060 ± 0.019	0.017 ± 0.005
1173	0.121 ± 0.025	0.065 ± 0.013
1273	0.151 ± 0.036	0.099 ± 0.024
1373	0.110 ± 0.031	0.080 ± 0.023

that has just been determined, Eq. (4.9), and the mobility ratio $b = u_n/u_p$ from Eq. (3.7) with the values for both $a^*_{O_2}$ and $a^o_{O_2}$ values in Tables 1 and 3. One can, thus, evaluate each mobility separately as summarized in Table 5, which is plotted in Fig. 14. Again disregarding the datum at 800°C, one may conclude that each mobility is very insensitive to temperature as has already been recognized in Fig. 14. Each mobility may be best estimated as

$$\begin{aligned} u_n/\mathrm{cm}^2\ \mathrm{V}^{-1}\ \mathrm{s}^{-1} &= 0.13 \pm 0.02; \\ u_p/\mathrm{cm}^2\ \mathrm{V}^{-1}\ \mathrm{s}^{-1} &= 0.081 \pm 0.017 \end{aligned} \tag{4.10}$$

in the temperature range of $1173 \leq T/K \leq 1373$. The mobility ratio turns out to be $b = 1.6$. In the literature [47], it was assumed to be $1 < b < 3$ over the similar temperature range, which fortuitously encloses the present value. It is here emphasized that the mobilities of electrons and holes have now been evaluated separately without having recourse to any assumption at all for the first time in the history of $BaTiO_3$ research.

4.3.3. Acceptor Concentration and Reduction Equilibrium Constant. The evaluated parameters, Eqs. (4.9) and (4.10), further enable one to determine the reduction equilibrium constant, K_{Re} in Eq. (2.1) and the concentration of the effective acceptors, $[\mathrm{A}']$ in Eq. (2.7). As $\sigma_n = \sigma_{\mathrm{el}}/(1+\alpha) = neu_n$, [see Figs. 4(a) and 5] one can evaluate "n" against oxygen activity by using Eqs. (4.10). The result is shown in Fig. 15. It is seen that as a_{O_2} decreases, the electron concentration gradually deviates from $n \propto a_{O_2}^{-1/4}$ (to a smaller exponent) at the temperatures except for 800°C. At 800°C, $n \propto a_{O_2}^{-1/4}$ essentially in the entire a_{O_2} range. Combining Eqs. (2.1), (2.3) and (2.8) and rearranging, one obtains a cubic equation with respect to "n",

$$a_{O_2}^{1/2} = \frac{2K_{\mathrm{Re}}}{n^2\left(n + [\mathrm{A}'] - \frac{K_i}{n}\right)} \tag{4.11}$$

The data in Fig. 15, except for 800°C, are NLLS fitted to this equation as depicted by the solid lines there. As is seen, the fitting is sufficiently precise. The fitting

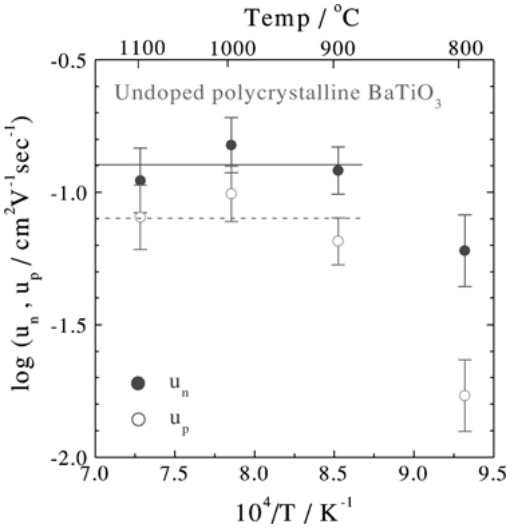

Fig. 14. Mobilities of electrons and holes, u_n and u_p, vs. reciprocal temperature for undoped $BaTiO_3$. The solid and dashed lines denote the average values of u_n, u_p, respectively, at temperatures, $1173 \leq T/K \leq 1373$.

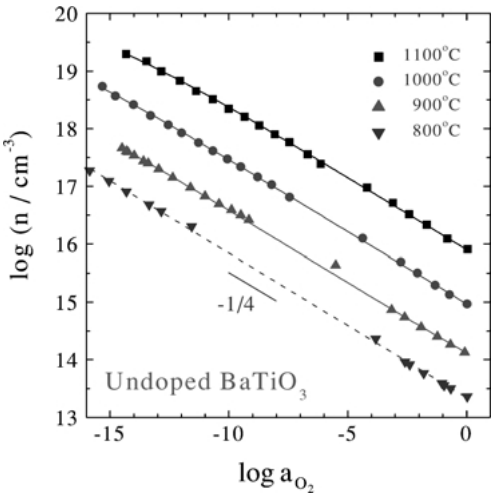

Fig. 15. Electron density n vs. oxygen activity at different temperatures. The solid lines are the best-fitted to Eq. (4.11) in the text. At 800°C, the entire range of oxygen activity belongs to the disorder regime ($V_O^{\bullet\bullet}, \mathrm{A}'$) where $m = 1/4$ and hence, Eq. (4.11) doesn't fit (i.e., a single line with a slope of $-1/4$).

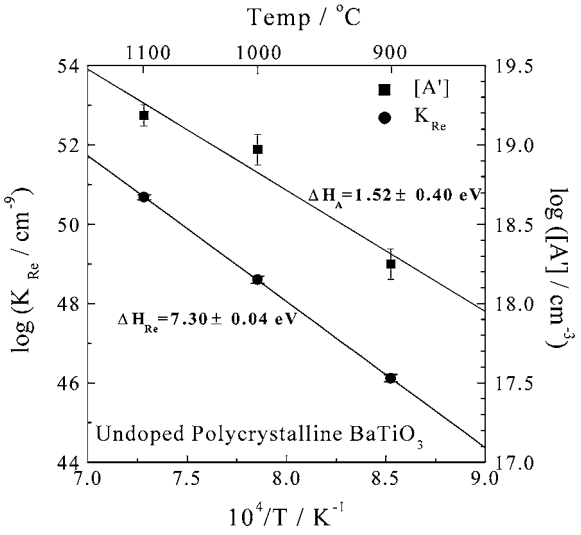

Fig. 16. Reduction equilibrium constant, K_{Re} and effective acceptor concentration, [A′] vs. reciprocal temperature. The solid lines are the best fitted.

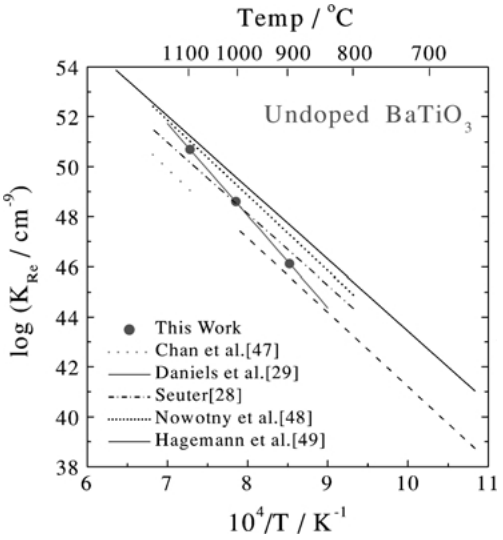

Fig. 17. Comparison of all the reported values for K_{Re} (Table 6 in the text).

parameters K_{Re} and [A′] are evaluated, respectively, as

$$[\mathrm{A}']/\mathrm{cm}^{-3} = \left(6.7^{+248}_{-6.5}\right) \times 10^{24} \times \exp\left(-\frac{1.52 \pm 0.40\ \mathrm{eV}}{kT}\right) \quad (4.12)$$

$$K_{\mathrm{Re}}/\mathrm{cm}^{-9} = \left(3.06^{+1.32}_{-0.91}\right) \times 10^{77} \times \exp\left(-\frac{7.30 \pm 0.04\ \mathrm{eV}}{kT}\right) \quad (4.13)$$

which are plotted in Fig. 16. It is surprising that the concentration of the effective acceptors, which has normally been regarded as constant in the literature [28, 29], turns out to be thermally activated, suggesting them being of intrinsic origin. For the 1.8 m/o Al-doped $BaTiO_3$ [14], on the other hand, the same procedure has yielded $[\mathrm{A}'] = 1.7 \times 10^{20}$ cm^{-3} or 1.1 m/o, that is in good agreement with the nominal value 1.8 m/o, and

$$K_{\mathrm{Re}}/\mathrm{cm}^{-9} = \left(2.40^{+10.4}_{-1.95}\right) \times 10^{74} \times \exp\left(-\frac{5.88 \pm 0.17\ \mathrm{eV}}{kT}\right) \quad (4.14)$$

All the values for K_{Re} reported on "undoped" $BaTiO_3$ along with the present one are listed in Table 6 and compared as shown in Fig. 17. One can see that the present value for the "undoped" $BaTiO_3$, Eq. (4.13) is not quite in agreement with the reported: Its activation energy and pre-exponential factor are $\Delta H_{\mathrm{Re}} = 7.3$ eV and $K^o_{\mathrm{Re}} \approx 10^{77}$ cm^{-9}, respectively, whereas the reported values are $\Delta H_{\mathrm{Re}} \approx 6$ eV and $K^o_{\mathrm{Re}} \approx 10^{71-73}$ cm^{-9}. For the 1.8 m/o Al-doped case, however, the corresponding

Table 6. Comparison of K_{Re} values reported on undoped $BaTiO_3$.

Author(s)	$K_{\mathrm{Re}}/\mathrm{cm}^{-9}$	Defect model	Measurement	Ref.
Chan et al.	$7.09 \times 10^{70} \exp(-\frac{5.89\,\mathrm{eV}}{kT})$	$n + [\mathrm{A}'_{\mathrm{C}}] = 2[\mathrm{V}^{\bullet\bullet}_{\mathrm{O}}]$	Conductivity, $u_n/u_p = 2$, u_n in Ref. 73	[47]
Seuter	$1.30 \times 10^{72} \exp(-\frac{5.70\,\mathrm{eV}}{kT})$	$[\mathrm{V}''_{\mathrm{Ba}}] = [\mathrm{V}^{\bullet\bullet}_{\mathrm{O}}]$	Conductivity, $u_n = 80$ T^{-1} cm^2 V^{-1}sec^{-1}	[28]
Daniels and Härdtl	$2.56 \times 10^{71} \exp(-\frac{6.10\,\mathrm{eV}}{kT})$	$[\mathrm{V}''_{\mathrm{Ba}}] = [\mathrm{V}^{\bullet\bullet}_{\mathrm{O}}]$	Conductivity, $u_n = 0.1$ cm^2 V^{-1} sec^{-1}	[29]
Nowotny and Rekas	$1.06 \times 10^{71} \exp(-\frac{5.69\,\mathrm{eV}}{kT})$	$n = 2[\mathrm{V}^{\bullet\bullet}_{\mathrm{O}}]$	Conductivity, u_n in Ref. 73	[48]
Hagemann and Hennings	$9.43 \times 10^{72} \exp(-\frac{5.99\,\mathrm{eV}}{kT})$	$n = 2[\mathrm{V}^{\bullet\bullet}_{\mathrm{O}}]$	Nonstoichiometry	[49]
Yoo and Song	$3.06 \times 10^{77} \exp(-\frac{7.30\,\mathrm{eV}}{kT})$	$n + [\mathrm{A}'] = 2[\mathrm{V}^{\bullet\bullet}_{\mathrm{O}}] + p$	Conductivity, chemical diffusivity	[50]

enthalpy is 5.88 eV (Eq. (4.14)), that is in excellent agreement with the literature values. It is noted that, in order to evaluate K_{Re} as defined in Eq. (2.1), one should know the absolute values for both n and $[V_O^{\bullet\bullet}]$. These can be directly determined, if exclusively in the disorder regime (e', $V_O^{\bullet\bullet}$), by measuring the oxygen nonstoichiometry. Otherwise, one would have to evaluate n from σ_n by using an appropriate value for u_n, and $[V_O^{\bullet\bullet}]$ on the basis of an appropriate defect model. In most of earlier works [28, 29, 47, 48], authors simply assumed the u_n-values or employed the values from different sources, thus highly likely lacking in the internal consistency between the values for σ_n and u_n used. In the present analysis, on the contrary, certainly is secured the internal consistency. Also, in the earlier works [28, 29], $[V_O^{\bullet\bullet}]$ was simply taken as constant in the regime (A', $V_O^{\bullet\bullet}$) because $[A']$ was presumed to be fixed as is the case with the Al-doped $BaTiO_3$. In the present analysis, however, $[A']$ has turned out to be thermally-activated with an activation enthalpy of $\Delta H_A = 1.5 \pm 0.4$ eV.

It seems to be not only fortuitous that $\Delta H_{\mathrm{Re}} - \Delta H_{\mathrm{A}} = 7.3 - 1.5 = 5.8$ eV is quite close to the reported ΔH_{Re} values ($\sim$6 eV) or the authors' own value for the Al-doped, 5.88 eV (Eq. (4.14)). By using the experimental values for $a^o_{O_2}$ (Table 3) and K_i (Eq. (4.9)), one obtains from Eq. (2.13)

$$2K_{\mathrm{Re}}/[A']/\mathrm{cm}^{-6} = \left(3.9^{+125.8}_{-3.8}\right) \times 10^{52} \times \exp\left(-\frac{5.71 \pm 0.33\ \mathrm{eV}}{kT}\right) \quad (4.15)$$

If one had simply assumed $[A']$ being temperature-independent, then one would have ended up with a reduction enthalpy of $\Delta H_{\mathrm{Re}} = 5.71$ eV, which is indeed in good agreement with the literature values in Table 6. Considering the internal consistency of the present analysis, it is, therefore, hard to deny the truthfulness of Eqs. (4.12) and (4.13) in the absence of evidence to the contrary.

4.3.4. Oxidation Equilibrium Constant. Once the reduction equilibrium constant, Eq. (4.14) is accepted, the oxidation equilibrium constant of undoped $BaTiO_3$ may be evaluated, which has never been attempted explicitly in literatures. One combines Eqs. (2.1) and (2.3), to obtain the oxidation reaction equilibrium

$$\frac{1}{2}O_2(g) + V_O^{\bullet\bullet} = O_O^x + 2h^{\bullet}; \quad K_{\mathrm{Ox}} = p^2[V_O^{\bullet\bullet}]^{-1}a_{O_2}^{-1/2} \quad (4.16)$$

where

$$K_{\mathrm{Ox}} = K_i^2 K_{\mathrm{Re}}^{-1}; \quad \Delta H_{\mathrm{Ox}} = 2\Delta H_i - \Delta H_{\mathrm{Re}} \quad (4.17)$$

Due to Eqs. (4.9) and (4.13), one, thus, obtains $\Delta H_{\mathrm{Ox}} = 2(3.15) - (7.30) = -1.06$ eV for the "undoped" $BaTiO_3$. For the 1.8 m/o Al-doped system, on the other hand, $\Delta H_{\mathrm{Ox}} = 2(2.15) - (5.88) = -1.58$ eV [14]. No doubt these values are negative, indicating the oxidation reaction is exothermic in perfect agreement with the nonstoichiometry measurement, see Section 6.

Looking back at the literature [18, 28, 29, 47–49], the defect chemical parameters, K_i and K_{Re} were evaluated mostly from the electrical conductivity isotherms, see Tables 4 and 6. In this case, one had to assume the values for the mobility of electronic carriers. Unless the consistent values for the mobilities were used, it would be likely to get ambiguous result. For undoped $BaTiO_3$, it was reported that $\Delta H_i = 2.9$–3.2 eV (Table 4) and $\Delta H_{\mathrm{Re}} = 5.7$–$6.1$ eV (Table 6). By combining these values, one would get a value for ΔH_{Ox} in the range of -0.3 – $+0.6$ eV. Even without taking into account the uncertainty of those enthalpy-values reported, thus, one cannot unequivocally say that the oxidation enthalpy is negative: it looks rather positive, being absolutely inconsistent with the nonstoichiometry variation with temperature, see Section 6. This seems to be the reason why the oxidation enthalpy has not been evaluated explicitly in the literature.

4.3.5. Nature of Effective Acceptors. What will then be A'? According to Eq. (4.12), $[A']$ decreases from 0.102 m/o at 1100°C to 0.062 m/o at 1000°C to 0.012 m/o at 900°C. These values are all much higher than the overall concentration of non-volatile impurities of the starting powder, $BaTiO_3$ (99.995% pure, Aldrich, U.S.A.), 6 ppm, of the specimens employed in the authors' own work. It is, thus, implied that the unidentified acceptors may be of intrinsic origin. The ionic conductivity at 800°C being higher than the extrapolated from the higher temperatures in Figs. 7 or 8 further suggests that these intrinsic acceptors may have been frozen-in somewhere between 900°C and 800°C.

As possible intrinsic acceptors, one may consider cation vacancies, V''_{Ba} and/or V''''_{Ti}. The situation, $[V^{\bullet\bullet}_O] \approx [V''_{Ba}]$ or $[V^{\bullet\bullet}_O] \approx 2[V''''_{Ti}]$, however, will be unlikely in the present case. It is because these types of majority disorder can be established only by nonmolecularity (ξ) or deviation from the ideal cation ratio ($[Ba^x_{Ba}]/[Ti^x_{Ti}] = 1$), and the nonmolecularity would have to be independent of temperature unless the stability limit with respect to ξ of $Ba_{1+\xi}TiO_{3-\delta}$ were crossed. (If the latter changed in the course of measurement, the chemical diffusivity would not be that high as shown in Fig. 10 because nonmolecularity reequilibration kinetics involves cation diffusion that is orders of magnitude smaller than that of oxygen, and then, the isotherms in Fig. 4 would not have been reproducible.) The next possibility of being thermally activated with nonmolecularity fixed may therefore be $[V^{\bullet\bullet}_O] \approx [V''_{Ba}] + 2[V''''_{Ti}]$ with $[V''_{Ba}] \approx [V''''_{Ti}]$, that is, the Schottky equilibrium with a negligible nonmolecularity ($\xi \approx 0$). This possibility has earlier been pointed out by Nowotny and Rekas [17], who argue that the cation vacancies, V''_{Ba} and V''''_{Ti}, should be prevailing for the specimen involving acceptor impurities of no greater than 10 ppm. But, it is also unlikely for the kinetic reason discussed above. Furthermore, even if it were the case, one would obtain an energy of $5\Delta H_A = 7.6$ eV for the Schottky defect formation enthalpy (see Eq. (2.4)), which is, however, too small compared to the theoretical value $\Delta H_S = 11.5$ eV by computer simulation [18]. The remaining possibility might then be anti-Frenkel disorder or $[A'] = 2[O''_i]$, which has never been thought of in a perovskite structure. If it is the case, nevertheless, one will have an energy of $2\Delta H_A = 3.0$ eV as the anti-Frenkel disorder formation energy. It is interesting to see the circumstantial evidences being accumulated which support the anti-Frenkel disorder as the majority type of ionic defects in perovskites [51–54]. In any case, the effective acceptors A' still remain unidentified tantalizingly.

4.3.6. Diffusivity of Oxygen Vacancies. Finally and for the sake of completeness, we evaluate the diffusivity of $V^{\bullet\bullet}_O$ from Eq. (3.4) by using Eq. (3.11) and Eq. (4.12) with the limiting neutrality condition, $2[V^{\bullet\bullet}_O] \approx [A']$. The results at 900°, 1000°, and 1100°C are shown in Fig. 18, where those of the 1.8 m/o Al-doped are also shown for comparison. The oxygen vacancy diffusivity turns out to be very insensitive to temperature: the average value is $D_{V_O} = 1.1 \times 10^{-5}$ cm^2 sec^{-1} as depicted by a solid line. Even though its magnitude looks

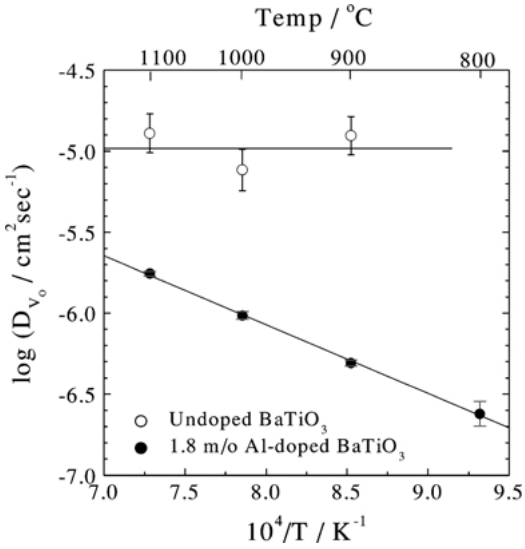

Fig. 18. log D_{V_O} vs. reciprocal temperature. The solid lines denote the average value for the undoped and the best fitted for 1.8 m/o Al-doped $BaTiO_3$.

reasonable in this temperature range, it is hard to accept the fact that D_{V_O} is little dependent on temperature.

One may argue that this result may likely be due to the error being enlarged upon propagation through the successive, multiple NLLS fitting processes, Eqs. (3.8), (4.7) and (4.11) for the evaluation of D_{V_O} via the Nernst-Einstein equation, Eq. (3.4). But, it may not necessarily be the entire reason: Shirasaki et al. [39] reported that the activation energy of oxygen tracer diffusion of undoped, polycrystalline $BaTiO_3$ in the atmosphere of $a_{O_2} = 0.05$ is only about 0.46 eV in the temperature range of $1043 \leq T/K \leq 1703$, see Fig. 9.

Such a small activation energy may render the self diffusivity of oxygen to appear temperature-insensitive over as small a temperature range as now. If the oxygen vacancy concentration of their specimens was fixed by background acceptor impurities or $[V^{\bullet\bullet}_O] \approx [A'_C]/2$, then the oxygen vacancy diffusion coefficient would also appear temperature-insensitive, say, D_{V_O} at 1100°C be larger than that at 900°C only by a factor of 2 (that is only 0.3 in a logarithmic scale). If it is the case, then it will be hard to differentiate within the error bound given in Fig. 18. It is also suggestive that for the 1.8 m/o Al-doped $BaTiO_3$ [14], exactly the same analysis has yielded an activation enthalpy for the vacancy diffusion as 0.84 eV in agreement with the literature [47, 55–57]. The answer to this problem seems to be with the nature of the effective acceptor, A'.

5. Thermoelectric Power

5.1. Compilation of Data

Reported data on the thermopower of $BaTiO_3$, be it undoped or doped, are extremely sparse compared to the electrical conductivity and chemical diffusivity. The very first was by Gerthsen et al. [58], who measured the thermopower in a temperature range of $1173 \leq T/K \leq 1523$ at a reducing atmosphere (75% N_2 + 25% H_2) only to confirm from the sign of thermopower that the major charge carriers of their specimen are electrons under the given thermodynamic condition. The complete thermopower isotherms, along with the corresponding conductivity isotherms, were first documented on undoped $BaTiO_3$ by Seuter [28] over a range of oxygen partial pressure in a temperature range of $1144 \leq T/K \leq 1397$. It was here first observed that the thermopower changes its sign crossing the oxygen partial pressure where the electrical conductivity becomes minimum and hence, the n-to-p transition has been confirmed. Recently, thermopower isotherms have been reported on single crystal $BaTiO_3$ in the ranges of $1090 \leq T/K \leq 1310$ and $10^{-15} \leq a_{O_2} \leq 1$ by Nowotny et al. [30], and on polycrystalline $BaTiO_3$, over the ranges of $1273 \leq T/K \leq 1473$ and $10^{-19} \leq a_{O_2} \leq 1$ by Kim et al. [16]. Among those reported, only the data available against oxygen partial pressure are compiled at, e.g., 1000°C in Fig. 19 where the authors' own (not corrected yet with respect to the type of atmosphere gas mixture, see Eq. (5.20) below) are also included.

The authors have measured the absolute thermopower on the same specimens of "undoped" $BaTiO_3$ on which the electrical conductivity [Section 3] and chemical diffusivity [Section 4] were earlier determined. The measured thermopower is the so-called "steady-state" thermopower of the system, namely the thermopower of the system $BaTiO_{3-\delta}$ that is in equilibrium with the local atmosphere gas in the surrounding along a temperature gradient applied and thus, subjected to a steady state nonstoichiometry gradient established (i.e., $\nabla\delta \neq 0$). Surrounding oxygen activity was controlled by O_2/N_2 gas mixtures for higher oxygen activities (e.g., $\log a_{O_2} > -5$ at 1000°C) and CO/CO_2 gas mixtures for lower oxygen activities (e.g., $\log a_{O_2} < -7$). For experimental details, the reader is referred to Ref. 12.

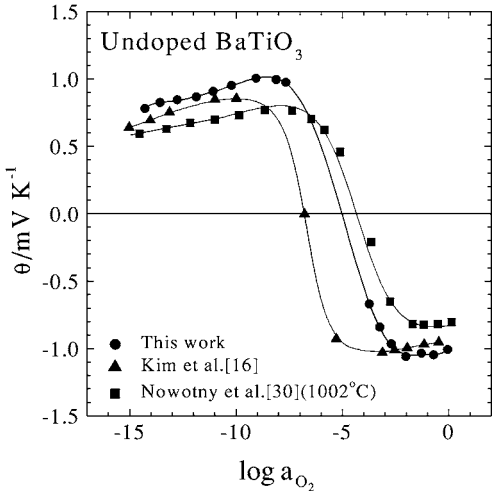

Fig. 19. Compilation of thermoelectric powers of undoped $BaTiO_3$ vs. oxygen activity at 1000°C.

One can see in Fig. 19 that the thermopower of undoped $BaTiO_3$ varies in an inverted S-shape against oxygen partial pressure, changing its sign at a specific oxygen partial pressure at a given temperature. This sort of S-shaped variation of thermopower as measured with electronic probes (normally Pt) is typical of the n-to-p transition and has also been reported on TiO_2[8], MnO[6], $La_{1-x}Sr_xFeO_3$ [59, 60], $Y_{1-x}Ca_xFeO_3$[34], and $LaCo_{0.2}Fe_{0.8}O_3$[61] among others.

The data sets of thermopower previously reported on $BaTiO_3$ [16, 28, 30, 58] were all analyzed in association with the corresponding electrical conductivity, if available, to estimate the type or density of electronic carriers on the basis of the formalism proposed by Jonker [62] and Becker and Frederikse [33]. These formalisms take account of only electrons and holes as charge carriers as in a classical, n/p mixed semiconductor. As is now clear from Fig. 6 or Table 1, $BaTiO_3$ is a mixed ionic electronic conductor. Therefore, its thermoelectric power should be a combination of the ionic and electronic contributions, and each is determined by the partial molar entropy and heat of transport of the respective type of carriers as is seen below. To date, the heat of transport has not been so well understood theoretically as well as experimentally [63]. It would thus not always be straightforward to evaluate the electronic carrier densities of $BaTiO_3$ from its overall thermopower without paying due attention to the heats of transport of electrons and holes as well as to the ionic contribution.

5.2. *Correlation with Defect Structure*

In the system of present interest, the mobile charged components are oxide anions (O^{2-}) and electrons (e^-). The absolute thermopower, θ, is then given as the sum of fractional contributions by each charged component [64, 65] or

$$\theta = t_{\rm el}\theta_{\rm el} + t_{\rm ion}\theta_{\rm ion} \tag{5.1}$$

In the light of linear irreversible thermodynamics, one can easily derive the electronic thermopower in terms of electronic carriers, electrons and holes as [64]

$$\theta_{\rm el} = \frac{1}{\rm e}\left[\frac{\sigma_n}{\sigma_n+\sigma_p}\left(\bar{S}_n + \frac{q_n^*}{T}\right) - \frac{\sigma_p}{\sigma_n+\sigma_p}\left(\bar{S}_p + \frac{q_p^*}{T}\right)\right] \tag{5.2}$$

Here, $\bar{S}_k$ stands for the partial molar entropy of species k and q_k^* the (reduced) heat-of-transport which is one of the least understood quantities in irreversible thermodynamics [63]. In this formulation, the potential at the higher temperature is taken as positive in accord with Wagner [64], leading to a positive sign of thermopower for a normal n-type semiconductor, contrary to semiconductor literatures. [33, 62]

The internal electronic excitation equilibrium or Eq. (2.3) presupposes

$$\begin{aligned} \eta_n + \eta_p = \mu_n + \mu_p = 0 \quad \text{or} \\ T(\bar{S}_n + \bar{S}_p) = \bar{H}_n + \bar{H}_p = \Delta H_i \end{aligned} \tag{5.3}$$

and the Boltzmann approximations regarding the partial molar entropies of the electronic carriers

$$\bar{S}_n = \bar{S}_n^o - k\ln n; \quad \bar{S}_p = \bar{S}_p^o - k\ln p \tag{5.4}$$

One can thus rewrite Eq. (5.2) in terms of the conductivity ratio α and mobility ratio b (in Eq. (3.2)) as

$$\theta_{\rm el} = -\frac{1}{2e}\left[\frac{\Delta H_i + q_n^* + q_p^*}{T}\tanh\left(\frac{1}{2}\ln\alpha\right) - k\ln(\alpha b) - \left(\bar{S}_n^o - \bar{S}_p^o + \frac{q_n^* - q_p^*}{T}\right)\right] \tag{5.5}$$

This equation is essentially identical to what have earlier been derived by Jonker [62] and Becker and Frederikse [33].

Equation (5.5) is generally valid irrespective of the type of majority disorder in Figs. 1 or 2. Particularly in the disorder regime of (n, $V_O^{\bullet\bullet}$) in Fig. 2, Eq. (5.5) reduces to the thermopower of an exclusively n-type semiconductor due to Eq. (3.5) or $\alpha \ll 1$, or

$$\theta_{\rm el} \approx \theta_n = \frac{1}{e}\left(-k\ln n + \bar{S}_n^o + \frac{q_n^*}{T}\right) \tag{5.6}$$

This has often been employed to estimate the density of carrier electrons n for an n-type semiconductor with appropriately assumed values for the standard entropy ($\bar{S}_n^o$) and heat of transport (q_n^*) of electrons. But, it should be pointed out that the uncertainties associated with these two quantities are exponentially propagated up to the electron density, n. For the present system, one can also recognize, due to Eq. (2.9), that

$$\left(\frac{\partial(e\theta_{\rm el}/k)}{\partial\ln a_{O_2}}\right)_T = \frac{1}{6} \tag{5.7}$$

For this reason, thermopower has been employed to determine the oxygen exponent m (see Eq. (3.9)) [30], but this practice cannot be justified unless either $\alpha \ll 1$ or $\alpha \gg 1$.

In the disorder regime of ($V_O^{\bullet\bullet}$, A'), one may use Eq. (3.6) to rewrite Eq. (5.5) in terms of oxygen activity as

$$\theta_{\rm el} = -\frac{1}{2e}\left[\frac{\Delta H_i + q_n^* + q_p^*}{T}\tanh\left(\frac{1}{4}\ln\frac{a_{O_2}}{a_{O_2}^*}\right) - \frac{1}{2}k\ln\frac{a_{O_2}}{a_{O_2}^*} - k\ln b - \left(\bar{S}_n^o - \bar{S}_p^o + \frac{q_n^* - q_p^*}{T}\right)\right] \tag{5.8}$$

The ionic contribution, $\theta_{\rm ion}$, on the other hand, is given as [64, 66]

$$\theta_{\rm ion} = \frac{1}{2e}\left(\frac{d\mu_O}{dT} + \bar{S}_{O^{2-}} + \frac{q_{O^{2-}}^*}{T}\right) \tag{5.9}$$

The ionic thermopower is dependent not only on the partial molar entropy $\bar{S}_{O^{2-}}$ and the heat-of-trasnsport $q_{O^{2-}}^*$ of oxide ions, but also on the distribution of the chemical potential of component oxygen, μ_O, along the temperature gradient applied. As μ_O is a function of T and δ for the system of $Ba_{1+\xi}TiO_{3+\delta}$ assuming that

the cation composition or nonmolecularity (ξ) remains homogeneously fixed, one may write

$$\frac{d\mu_{\mathrm{O}}}{dT} = \left(\frac{\partial \mu_{\mathrm{O}}}{\partial T}\right)_{\delta} + \left(\frac{\partial \mu_{\mathrm{O}}}{\partial \delta}\right)_{T} \frac{d\delta}{dT} = -\bar{S}_{\mathrm{O}} + W \tag{5.10}$$

It is noted that the partial molar entropy of component oxygen, $\bar{S}_{\mathrm{O}}$, depends on gas mixtures employed to control the oxygen activity in the surrounding of an oxide system assuming gas/solid oxygen exchange equilibrium prevailing as is the case with the present $Ba_{1+\xi}TiO_{3+\delta}$ in steady state at elevated temperatures [12]. The oxygen activity in the surrounding is normally controlled by O_2/inert gas (e.g. N_2) mixtures and/or CO_2/CO gas mixtures. In the former a_{O_2} is fixed and in the latter the mixing ratio $r(= P_{CO_2}/P_{CO})$ is fixed. One, thus, obtains:

(i) In O_2/N_2 atmospheres,

$$-\bar{S}_{\mathrm{O}} = -\frac{1}{2}S^{o}_{O_2} + \frac{1}{2}k \ln a_{O_2} \tag{5.11}$$

due to

$$\mu_{\mathrm{O}(S)} = \frac{1}{2}\mu_{O_2(g)} \tag{5.12}$$

(ii) In CO_2/CO atmospheres:

$$\begin{aligned} -\bar{S}_{\mathrm{O}} &= -S^{o}_{CO_2} + S^{o}_{CO} + k \ln r \\ &= -\frac{1}{2}S^{o}_{O_2} - \frac{\Delta H^{o}_{g}}{T} + \frac{1}{2}k \ln a_{O_2} \end{aligned} \tag{5.13}$$

due to the reaction equilibrium $CO + \frac{1}{2}O_2 = CO_2$ or

$$\mu_{\mathrm{O}} = \frac{1}{2}\mu_{O_2(g)} = \mu_{CO_2} - \mu_{CO} \tag{5.14}$$

where ΔH^{o}_{g} is the standard enthalpy of the reaction, -282.4 kJ/mol [67].

The thermodynamic factor W in Eq. (5.10) depends on the distribution of oxygen nonstoichiometry along a temperature gradient applied. For the case of thin specimens of $BaTiO_{3-\delta}$ like those[4] used in the authors' own work [12], thermodynamic equilibrium with the local surrounding (T, a_{O_2}) are swiftly achieved due to the fast, gas/solid-equilibration kinetics as described in Section 4. Here we identify the factor only in the regime $(V_{\mathrm{O}}^{\bullet\bullet}, A')$ of the present concern. In this regime the oxygen nonstoichiometry δ, as defined as $BaTiO_{3-\delta}$, may be written, due to Eq. (4.5), as

$$\delta = \frac{V_m}{N_A}\left([V_{\mathrm{O}}^{\bullet\bullet}] - \frac{1}{2}[A']\right) = \frac{V_m}{N_A}\sqrt{K_i}\sinh\left(\frac{1}{4}\ln\frac{a_{O_2}}{a^{o}_{O_2}}\right) \tag{5.15}$$

Therefore, the thermodynamic factor W takes the form depending on the measurement conditions as:

(1) In a_{O_2} = fixed (N_2/O_2) atmospheres,

$$W = \frac{\Delta H_i}{T}\tanh\left(\frac{1}{4}\ln\frac{a_{O_2}}{a^{o}_{O_2}}\right) - \frac{\Delta H_{\mathrm{Re}} - \Delta H_A - \Delta H_i}{T} \tag{5.16}$$

(2) In $r =$ fixed (CO_2/CO) atmospheres, due to Eqs. (5.15) and (5.14),

$$W = \frac{\Delta H_i}{T}\tanh\left(\frac{1}{4}\ln\frac{a_{O_2}}{a^{o}_{O_2}}\right) - \frac{\Delta H_{\mathrm{Re}} - \Delta H_A - \Delta H_i + \Delta H^{o}_{g}}{T} \tag{5.17}$$

The steady state ionic thermopower of $BaTiO_3$ in the regime of $(V_{\mathrm{O}}^{\bullet\bullet}, A')$ is thus

(i) in O_2/N_2 atmospheres,

$$\begin{aligned} &\theta_{\mathrm{ion}}(O_2/N_2; \nabla\delta \neq 0) \\ &= \frac{1}{2e}\left\{-\frac{1}{2}S^{o}_{O_2} + \frac{1}{2}k\ln a_{O_2} + \bar{S}_{O^{2-}} + \frac{q^{*}_{O^{2-}}}{T} + \frac{\Delta H_i}{T}\right. \\ &\quad \left.\times\left[1 + \tanh\left(\frac{1}{4}\ln\frac{a_{O_2}}{a^{o}_{O_2}}\right)\right] - \frac{\Delta H_{\mathrm{Re}} - \Delta H_A}{T}\right\} \end{aligned} \tag{5.18}$$

(ii) in CO_2/CO atmospheres,

$$\begin{aligned} &\theta_{\mathrm{ion}}(CO_2/CO; \nabla\delta \neq 0) \\ &= \frac{1}{2e}\left\{-\frac{1}{2}S^{o}_{O_2} + \frac{1}{2}k\ln a_{O_2} + \bar{S}_{O^{2-}} + \frac{q^{*}_{O^{2-}}}{T} + \frac{\Delta H_i}{T}\right. \\ &\quad \times\left[1 + \tanh\left(\frac{1}{4}\ln\frac{a_{O_2}}{a^{o}_{O_2}}\right)\right] \\ &\quad \left. - \frac{\Delta H_{\mathrm{Re}} - \Delta H_A}{T} - \frac{2\Delta H^{o}_{g}}{T}\right\} \end{aligned} \tag{5.19}$$

Now, the absolute thermopower of $BaTiO_{3-\delta}$ in the disorder regime of $(A', V_O^{\bullet\bullet})$ can be evaluated by combining, via Eqs. (5.1), and (5.8) and either Eq. (5.18) or (5.19) depending on gas atmospheres. It is emphasized that if $t_{el} \gg t_{ion}$, the thermopower will be essentially independent of atmospheric gases and antisymmetrical against $\ln a_{O_2}$. Therefore, once the thermopower turns out to depend on the type of gas mixtures employed and/or to be non-antisymmetrical against $\ln a_{O_2}$, the ionic contribution will have to be non-negligible.

Finally, one can recognize from Eqs. (5.18) and (5.19) that the absolute thermopower as measured in a CO/CO_2 atmosphere differ from that measured in the corresponding O_2/N_2 atmosphere as

$$\theta(O_2/N_2; \nabla\delta \neq 0) = \theta(CO_2/CO; \nabla\delta \neq 0) + t_{ion}\frac{\Delta H_g^o}{eT} \tag{5.20}$$

5.3. *Defect-Chemical Analysis*

The steady state, absolute thermopowers as measured by the authors are shown in Fig. 20 for the "undoped" $BaTiO_3$(a) along with those for the Al-doped (b) for comparison. The data in the range of $\log a_{O_2} < -5$ were obtained in CO_2/CO atmospheres and the rest (in the range of $\log a_{O_2} > -5$) in O_2/N_2 atmospheres. As shown in Fig. 5, the almost entire range of a_{O_2} examined is enclosed in the defect regime of $(A', V_O^{\bullet\bullet})$. One can see that the thermopower isotherms appear to deviate somewhat from antisymmetry and the deviation becomes more appreciable as temperature is lowered. For the 1.8 m/o Al-doped, the asymmetry is more conspicuous, see Fig. 20(b). If the specimen were purely electronic or $t_{el} \gg t_{ion}$, then the isothermal variation of absolute thermopower against $\log a_{O_2}$ would be antisymmetrical as indicated by Eq. (5.8). This deviation from the anti-symmetry or a dependence on measurement atmospheres indicates that the ionic contribution is not totally negligible to the thermopower of present $BaTiO_3$.

The thermopowers as measured in CO_2/CO atmospheres are normalized to that of O_2/N_2 atmospheres via Eq. (5.20) by using the values for t_{ion} as determined in Fig. 6. The results are as shown in Fig. 21. The normalized thermopower may be represented by associating Eqs. (5.8) and (5.18) via

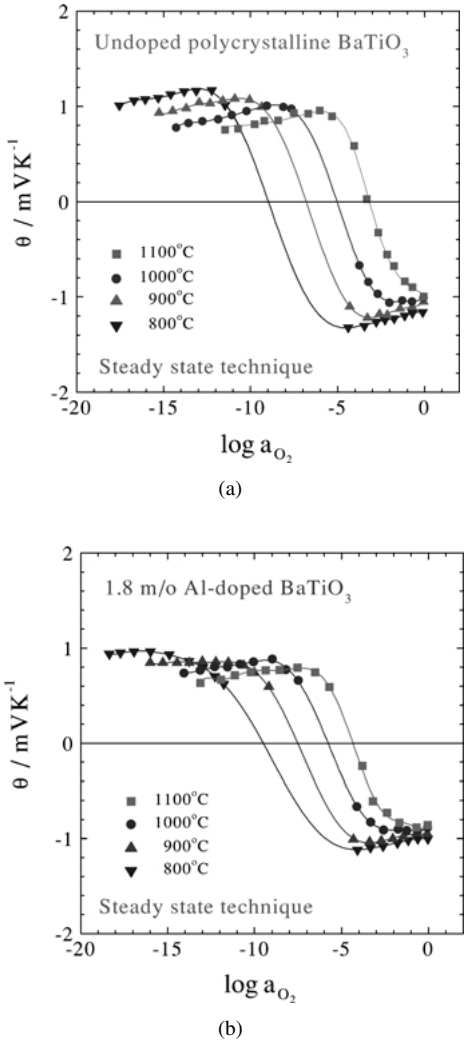

Fig. 20. As-measured isotherms of steady state (absolute) thermopower of (a) "undoped" and (b) 1.8 m/o Al-doped $BaTiO_3$. Note that the oxygen activity was controlled by N_2/O_2 gas mixtures for $\log a_{O_2} > -5$, and otherwise, CO/CO_2 gas mixtures. The solid lines are for visual guidance only.

Eq. (5.1) as

$$\frac{2e\theta}{k} = t_{ion}\left\{A + B\left[1 + \tanh\left(\frac{1}{4}\ln\frac{a_{O_2}}{a_{O_2}^o}\right)\right] + \frac{1}{2}\ln a_{O_2}\right\} - t_{el}\left[C\tanh\left(\frac{1}{4}\ln\frac{a_{O_2}}{a_{O_2}^*}\right) - \frac{1}{2}\ln\frac{a_{O_2}}{a_{O_2}^*} - \ln b + D\right] \tag{5.21}$$

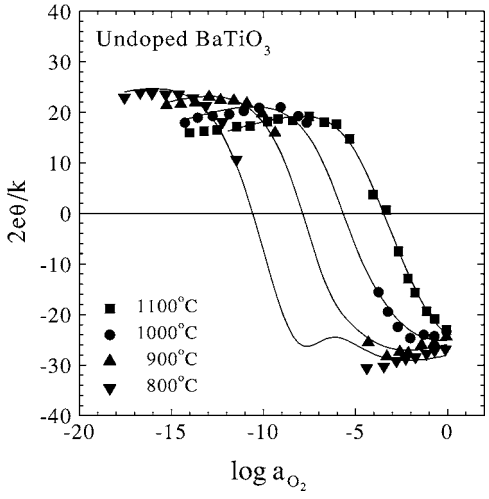

(a)

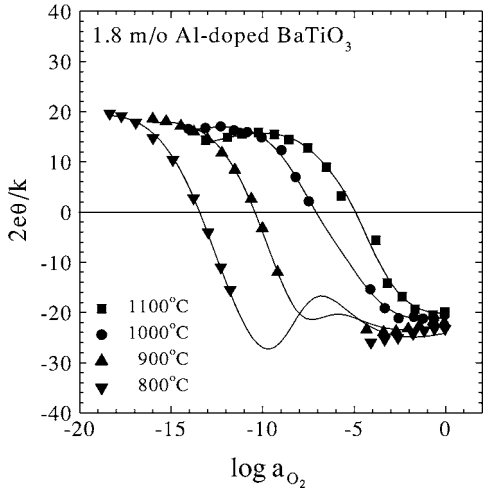

(b)

Fig. 21. Normalized thermopower isotherms of (a) undoped and (b) 1.8 m/o Al-doped $BaTiO_3$, respectively. The solid lines are the best fitted to Eq. (5.21) in the text.

where

$$A = -\frac{S^o_{O_2}}{2k} + \frac{\bar{S}_{O^{2-}}}{k} + \frac{q^*_{O^{2-}}}{kT} - \frac{\Delta H_{Re} - \Delta H_A}{kT};$$

$$B = \frac{\Delta H_i}{kT}; \quad C = \frac{\Delta H_i + q^*_p + q^*_n}{kT}; \qquad (5.22)$$

$$D = \frac{q^*_p - q^*_n}{kT} + \frac{\bar{S}^o_p - \bar{S}^o_n}{k}$$

In Sections 3 and 4, we evaluated t_{ion}, $a^o_{O_2}$, $a^*_{O_2}$, b, and ΔH_i (hence B) on the same specimens at each temperature. By using these values and assuming that the parameters A, C and D in Eq. (5.22) are insensitive to oxygen activity, we fit the normalized thermopower isotherms in Fig. 21 to Eq. (5.21). The results are as depicted by the solid lines in Fig. 21 and the fitting parameters A, C and D are evaluated as listed in Table 7. One may recognize that Eq. (5.21) explains the isotherms reasonably well.

Table 7. Parameters, A, C and D, evaluated from the isotherms of normalized thermopower for the undoped $BaTiO_3$.

T/K	A	C	D
1073	$-(59.0 \pm 6.2)$	36.86 ± 0.40	2.46 ± 0.57
1173	$-(68.2 \pm 5.9)$	33.19 ± 0.33	1.14 ± 0.47
1273	$-(48.0 \pm 5.4)$	31.01 ± 0.44	1.72 ± 0.57
1373	$-(5.0 \pm 3.2)$	30.45 ± 0.37	4.59 ± 0.50

It is noted that the ionic thermopower is expected to become more appreciable particularly in the vicinity of $a^o_{O_2}$ as the temperature is lowered, say at 900° and 800°C. The ionic humps there are due to the W-factor (Eq. (5.10)) increasing as a_{O_2} increases across $a^o_{O_2}$, and t_{ion} becoming maximum at $a^*_{O_2}$, that is close to $a^o_{O_2}$. Unfortunately, however, the actual observation could not be made because this oxygen partial pressure region was normally hard to realize experimentally. As a consequence any further quantitative analysis of the ionic thermopower cannot be made from the fitted values for A, and hence, the attention is drawn to the electronic part.

As the absolute thermopower in Fig. 21 is governed mostly by the electronic contribution ($t_{el} > 0.5$, see Fig. 6), the evaluated values for the electronic parameters C and D may be regarded as being relatively more reliable. One may, thus, take the difference "$C - B$" in Table 7 to evaluate the sum of the heats of transport, $q^*_p + q^*_n$ at each temperature, which has turned out to be temperature-insensitive and best estimated as

$$q^*_p + q^*_n = 0.26 \pm 0.11 \text{ eV} \qquad (5.23)$$

For the 1.8 m/o Al-doped, this value is 0.91 ± 0.06 eV, differing very much [12]. Assuming that the standard entropies of electronic carriers, $\bar{S}^o_p$ and $\bar{S}^o_n$, are insensitive to temperature, one may plot the parameter D against reciprocal temperature hopefully to determine the difference of the heats of transport, $q^*_p - q^*_n$. The results are as shown in Fig. 22, where the result for the 1.8 m/o Al-doped sample is also shown for comparison.

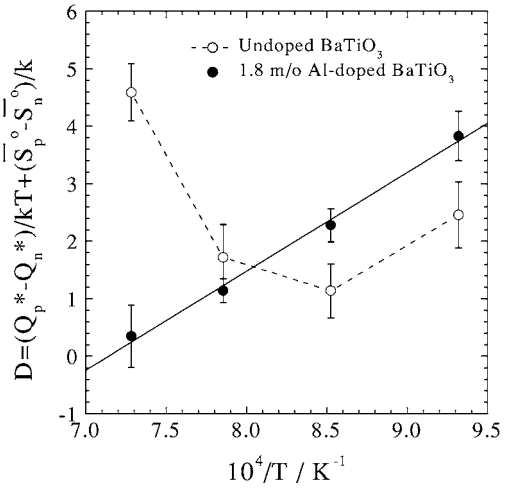

Fig. 22. The fitting parameters D (in Eq. (5.22) in the text) vs. reciprocal temperature for undoped (dashed line) and 1.8 m/o Al-doped $BaTiO_3$ (solid line). The dashed line is only for visual guidance and the solid line the best fit via linear regression.

The variation of D for the "undoped" specimen is in general quite different from that of the Al-doped, but the partial trend below 900°C looks quite similar to the doped. This seems to be not only fortuitous: The electrical conductivity and chemical diffusivity have strongly suggested that the defect structure of the same "undoped" specimen is of intrinsic nature and is frozen-in upon passing 900°C (see Figs. 8 and 12) and hence, the trend of the properties of the "undoped" specimen appears the same as that of the Al-doped below 900°C. Unlike the Al-doped, the difference between the heats of transport, thus, cannot be evaluated, and hence each heat of transport cannot be separated from Eq. (5.23).

Nevertheless, the result of Eq. (5.23) appears to be consistent with the mobilities of electronic carriers in Fig. 13, which suggest phonon scattering. In this case, $q_n^*, q_p^* \approx kT$ [33, 62, 68] or ≈0.1 eV, e.g., at 1273 K.

6. Nonstoichiometry

6.1. *Compilation of Data*

The nonstoichiometry δ of $BaTiO_{3-\delta}$ is a measure of oxygen deficit in the present context. There have thus far been reported on undoped $BaTiO_{3-\delta}$ five different data sets [28, 49, 69–71] against oxygen partial pressure in the range of $\log a_{O_2} < -7$ over the overall temperature range of 1000°C to 1340°C. But, only relative changes in nonstoichiometry were given [28, 70] or even when the absolute values were reported [49, 69, 71], the stoichiometric points could not be located seemingly due to limited precision. Without knowing the absolute values, one may not be able to grasp the quantitative, defect-chemical understanding of the nonstoichiometry.

In Fig. 23 are compiled all the reported data on nonstoichiometry of undoped $BaTiO_{3-\delta}$ [28, 49, 69–71] including the authors' own [13]. For the sake of compilation, the relative values reported [28, 70] have been simply regarded as the absolute ones. (Their reference points were $a_{O_2} = 0.1$ [28] and 0.21 [70], respectively, where the absolute nonstoichiometry values are actually very small compared to those shown in Fig. 23.) It is mentioned that all the reported except for Ref. 69, which was by colorimetry, were by thermogravimetry, and only authors' own data by coulometric titrometry.

Evaluation of the absolute values for nonstoichiometry is not a trivial task. One way is to locate an

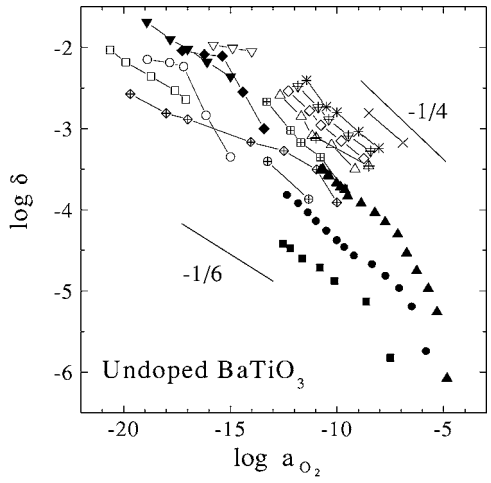

Fig. 23. Compilation of all the nonstoichiometry data reported on undoped $BaTiO_{3-\delta}$ including the authors' own [15]. Note that the data from Refs. 28 and 70 are the values relative to the atmospheres of $a_{O_2} = 0.1$ and 0.21, respectively; —○— Panlener et al. [70] 1000°C in-situ TGA, —◈— Hagemann et al. [49] 1000°C in-situ TGA, —⊕— Seuter [28] 1040°C in-situ TGA, —□— Bois et al. [69] 1050°C ex-situ colorimetric method, —◆— Panlener et al. [70] 1100°C in-situ TGA, —⊞— Hennings [71] 1115°C in-situ TGA, —△— Hennings [71] 1150°C in-situ TGA, —◇— Hennings [71] 1183°C in-situ TGA, —⊿— Seuter [28] 1200°C in-situ TGA, —▽— Panlener et al. [70] 1200°C in-situ TGA, —▼— Bois et al. [69] 1200°C ex-situ colorimetric method, —⊽— Hennings [71] 1216°C in-situ TGA, —✳— Hennings [71] 1250°C in-situ TGA, —×— Seuter [28] 1340°C in-situ TGA, ▲ (This work, 1000°C, ● This work, 900°C, ■ This work, 800°C) in-situ Coulometric titration.

inflection point on a nonstoichiometry isotherm which falls at the stoichiometric composition (be it either electronic or ionic stoichiometric composition) [72]. In order for it to include an inflection point in its range of variation, the isotherm should enclose not only an oxygen deficit branch ($\delta > 0$), but an oxygen excess one ($\delta < 0$) also. We have seen that undoped $BaTiO_{3-\delta}$ undergoes an n-type to p-type transition in its semi-conducting behavior at a a_{O_2} normally higher than 10^{-6} [See Figs. 3 and 4], indicating the presence of a stoichiometric composition ($\delta = 0$) nearby. It is, thus, necessary to extend the measurement on $BaTiO_3$ up to sufficiently high an oxygen partial pressure so that the electronic stoichiometric composition can be enclosed.

The authors have measured the oxygen nonstoichiometry of the "undoped" $BaTiO_{3-\delta}$ as a function of oxygen partial pressure in the range, $10^{-15} \leq a_{O_2} \leq 0.1$ enclosing the n-to-p transition point at 800, 900, and 1000°C, respectively. It is reminded that while the specimens for the study of electrical conductivity, chemical diffusivity and thermopower were from the same piece of sintered $BaTiO_3$, those for nonstoichiometry measurement were separately prepared later but from the same 99.995% purity Aldrich powder. In appearance, the latter differ from the former only in microstructure: ca. 90% of the theoretical density with an average grain size of 60 ± 20 μm, while the former of 94% density and 43 μm grain size. The measurements were essentially free from the influences of the possible artifacts associated with the coulometric titrometry such as mechanical leakage through joints between the titration cell components, electrochemical leakage through the electrolyte (YSZ) employed, chemical reactions between the sample and neighboring cell components, nonstoichiometry change of the electrolyte itself, etc. For experimental details, the reader is referred to Ref. 13.

6.2. *Correlation with Defect Structure*

On the basis of the defect structure discussed in Section 2, a lattice molecule of the system may be represented as

$$(\mathrm{Ba, Ti})_{2-x}(\mathrm{A}')_x O_{3-(x/2)-\delta} \tag{6.1}$$

and the nonstoichiometry δ, the deviation from the (electronic) stoichiometric composition ($\delta \equiv 0$) is given due to Eq. (4.5) as

$$\frac{N_A \delta}{V_m} = [\mathrm{V}_\mathrm{O}^{\bullet\bullet}] - \frac{1}{2}[\mathrm{A}'] = \frac{1}{2}(n - p) \tag{6.2}$$

By using Eqs. (2.1), (2.3) and (2.8), one thus obtains

$$\Delta\delta = \delta - \delta^* = -\frac{V_m}{N_A}\sqrt{K_i}\sinh\left[\frac{1}{2}\ln\left(1 + \frac{2N_A\delta}{V_m[\mathrm{A}']}\right) + \frac{1}{4}\ln\left(\frac{a_{\mathrm{O}_2}}{a^o_{\mathrm{O}_2}}\right)\right] - \delta^* \tag{6.3}$$

over the entire a_{O_2} ranges in Fig. 2. Particularly in the regime of $(\mathrm{V}_\mathrm{O}^{\bullet\bullet}, \mathrm{A}')$ where $2N_A\delta/V_m \ll [\mathrm{A}']$, this equation reduces to

$$\Delta\delta = \delta - \delta^* = -\frac{V_m}{N_A}\sqrt{K_i}\sinh\left[\frac{1}{4}\ln\frac{a_{\mathrm{O}_2}}{a^o_{\mathrm{O}_2}}\right] - \delta^* \tag{6.4}$$

Here δ^* denotes the nonstoichiometry value that the specimen initially has before starting coulometric titration. What can be experimentally measured is thus $\Delta\delta = \delta - \delta^*$.

6.3. *Defect Chemical Analysis*

The nonstoichiometry varies against $\log a_{O_2}$ as shown in Fig. 24. Upon comparison with Fig. 5, one can recognize that the a_{O_2}-range examined does essentially belong to the disorder regime of $(\mathrm{V}_\mathrm{O}^{\bullet\bullet}, \mathrm{A}')$. The raw data, thus, have been best fitted to Eq. (6.4) as depicted by the solid curves in Fig. 24. As is seen, Eq. (6.4) describes the nonstoichiometry quite precisely with the best estimated values for the fitting parameters, δ^*, K_i and $a^o_{\mathrm{O}_2}$ that are listed in Table 8.

The K_i values are plotted against reciprocal temperature in Fig. 25, which is best represented as

$$K_i/\mathrm{cm}^{-6} = \left(1.08^{+59.2}_{-0.02}\right) \times 10^{46} \times \exp\left(-\frac{2.82 \pm 0.39\ \mathrm{eV}}{kT}\right) \tag{6.5}$$

in the entire temperature range. K_i has earlier been evaluated in Section 4 (Eq. (4.9)), which is also shown in Fig. 25. We observed there that the value at 800°C is appreciably off the linear trend at the higher temperatures. One may likewise argue here that the datum

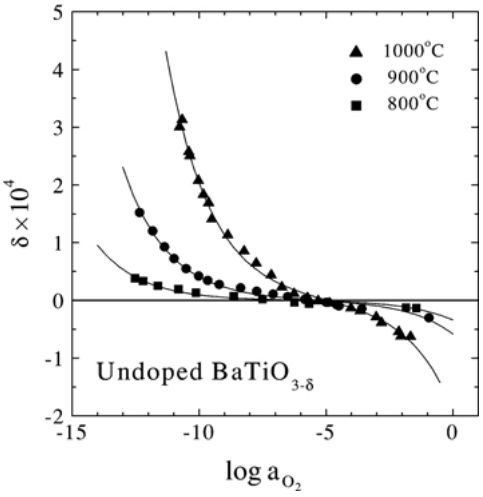

Fig. 24. Oxygen nonstoichiometry, δ vs. log a_{O_2} for undoped $BaTiO_{3-\delta}$ of 99.995% purity at different temperatures. The solid lines are the best fit to Eq. (6.4) in the text.

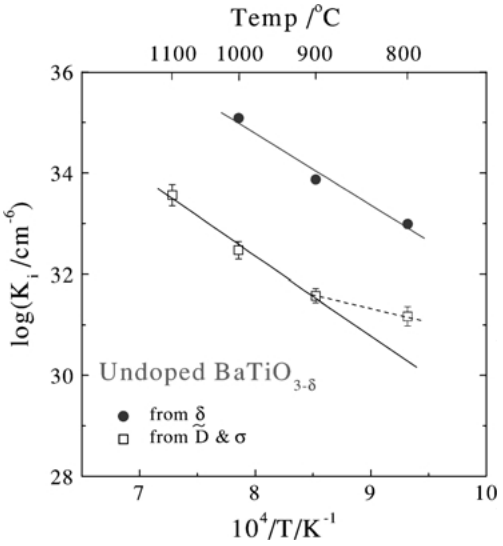

Fig. 25. Comparison of electronic equilibrium constants K_i extracted from chemical diffusivity and conductivity combined (Eq. (4.9)), and from nonstoichiometry, respectively.

at 800°C is also off the extrapolation from the high temperatures, but the number of data is too scarce. In any case, the present K_i values are 2 to 3 orders of magnitude larger than the corresponding values evaluated previously. The electronic stoichiometric points, $a^o_{O_2}$ of Table 8 are also compared with those obtained from $\tilde{D}$ in Table 3 in Fig. 26. Only at 1000°C, they are fortuitously in reasonable agreement with each other, but at the lower temperatures, the former values are 2–3 orders of magnitude larger. The reasons for these discrepancies are not immediately clear.

Nevertheless, we will finally document the partial molar quantities of component oxygen from the $\delta - a_{O_2} - T$ relation in Fig. 24. Due to the gas/solid equilibrium criterion, the relative partial molar Gibbs free energy of oxygen is written as

$$\Delta\bar{G}_O = \mu_{O(S)} - \frac{1}{2}\mu^o_{O_2(g)} = \frac{1}{2}RT \ln a_{O_2}. \qquad (6.6)$$

Table 8. The best estimated values for $\log K_i$, $\log a^o_{O_2}$, and δ^* by nonlinear fitting of Eq. (6.4) to the experimental data for 99.995% pure $BaTiO_{3-\delta}$.

	$\log(K_i/\mathrm{cm}^{-6})$	$\log a^o_{O_2}$	δ^*
1000°C	35.08 ± 0.04	$-(4.94 \pm 0.08)$	$-(6.3 \pm 0.3) \times 10^{-5}$
900°C	33.87 ± 0.04	$-(5.31 \pm 0.09)$	$-(3.0 \pm 0.1) \times 10^{-5}$
800°C	32.99 ± 0.04	$-(6.1 \pm 0.2)$	$-(1.5 \pm 0.2) \times 10^{-5}$

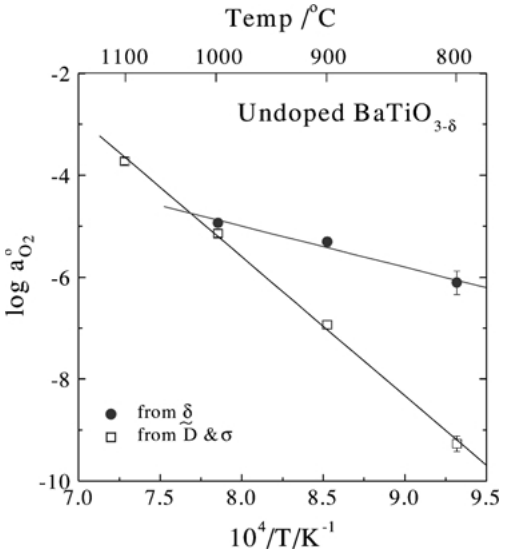

Fig. 26. Comparison of $\log a^o_{O_2}$ extracted from chemical diffusivity (Table 3) and nonstoichiometry, respectively.

The relative partial molar enthalpy, $\Delta\bar{H}_O$ and entropy, $\Delta\bar{S}_O$ of component oxygen are thus related to the equilibrium a_{O_2} as

$$\ln a_{O_2} = \frac{2\Delta\bar{H}_O}{RT} - \frac{2\Delta\bar{S}_O}{R} \qquad (6.7)$$

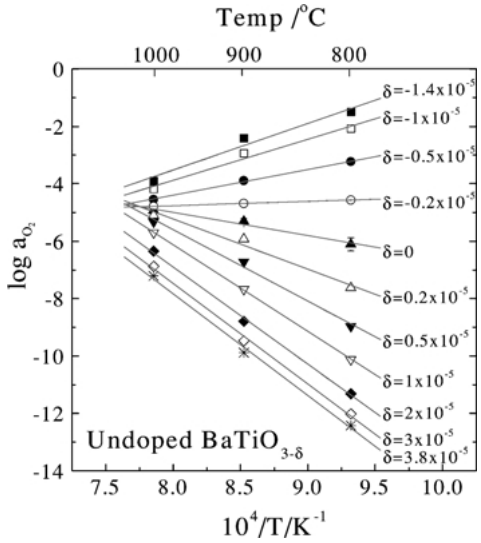

Fig. 27. Equilibrium oxygen activity vs. reciprocal temperature at different nonstoichiometries for undoped $BaTiO_{3-\delta}$ (99.995% purity).

In Fig. 27 is plotted log a_{O_2} vs. reciprocal temperature at different nonstoichiometries. As is seen, it is generally linear for a fixed δ over the temperature range examined. The relative partial molar enthalpy and entropy of oxygen may then be evaluated from the slope and intercept, respectively. The results are summarized in Figs. 28 and 29.

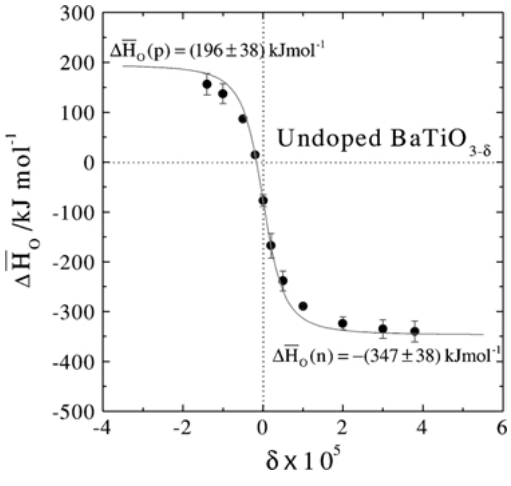

Fig. 28. Relative partial molar enthalpy, $\Delta\bar{H}_O$, of oxygen vs. nonstoichiometry δ. The solid curve is the calculated on the basis of the ideal dilute solution model, Eq. (6.11) in the text.

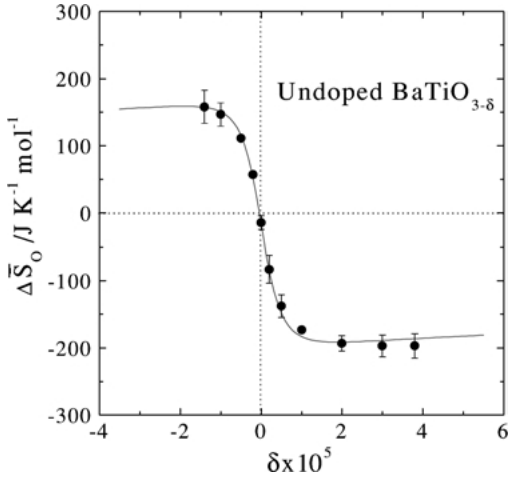

Fig. 29. Relative partial molar entropy, $\Delta\bar{S}_O$, of oxygen vs. nonstoichiometry δ. The solid curve is the calculated on the basis of the ideal dilute solution model, Eq. (6.15) in the text.

It is noted that as δ increases or $BaTiO_{3-\delta}$ becomes essentially n-type ($\delta \gg 0$ or $n \gg p$, see Fig. 5), $\Delta\bar{H}_O$ appears to saturate (to ca. -350 kJ mol^{-1}) and as δ crosses 0 or the oxide undergoes the n-to-p transition, $\Delta\bar{H}_O$ varies very rapidly. A similar trend is also observed with $\Delta\bar{S}_O$ crossing the stoichiometric composition. These rapid variations across $\delta = 0$ may be attributed to the difference in detailed oxygen incorporation reaction between the two branches of $BaTiO_{3-\delta}$, Eq. (4.15) and the reverse of Eq. (2.1), or

$$\frac{1}{2}O_2(g) + V_O^{\bullet\bullet} = O_O^{\times} + 2h^{\bullet}; \qquad (6.8)$$

$$\frac{1}{2}O_2(g) + V_O^{\bullet\bullet} + 2e' = O_O^{\times} \qquad (6.9)$$

in the mostly p-type (say, $\delta < -5 \times 10^{-5}$ or $p \gg n$) and n-type ($\delta > 5 \times 10^{-5}$ or $n \gg p$) branch, respectively. We presume the ideal dilute solution behavior of defects in the present system. The partial molar enthalpy of component oxygen will, thus, be independent of δ in each branch, say, $\delta > 5 \times 10^{-5}$ and $\delta < -5 \times 10^{-5}$ as expected from Fig. 28. According to Eqs. (6.8) and (6.9), the difference in the relative partial molar enthalpy of oxygen between the n and p branches should be $\Delta\bar{H}_O(p) - \Delta\bar{H}_O(n) = 2\Delta H_i = 543$ kJ/mol-O due to Eq. (6.5). (Here, we use the ΔH_i value in Eq. (6.5) rather than in Eq. (4.9) for the sake of internal consistency.) In the n-to-p transition regime, $\Delta\bar{H}_O$ may be given as the fractional sum of $\Delta\bar{H}_O(p)$ and $\Delta\bar{H}_O(n)$

or due to Eqs. (2.3) and (6.4),

$$\Delta\bar{H}_O = \frac{n}{n+p}\Delta\bar{H}_O(n) + \frac{p}{n+p}\Delta\bar{H}_O(p)$$
$$= \frac{1}{2}[\Delta\bar{H}_O(p) + \Delta\bar{H}_O(n)] - \frac{\beta\delta}{2[(\beta\delta)^2 + 4K_i]^{1/2}}$$
$$\times [\Delta\bar{H}_O(p) - \Delta\bar{H}_O(n)] \quad (6.10)$$

with $\beta \equiv 2N_A/V_m (= 3.14 \times 10^{22}\ \text{cm}^{-3})$. By using the value $K_i = 7.41 \times 10^{33}\ \text{cm}^{-6}$ at 900°C (see Table 8), Eq. (6.10) is fitted to the data as depicted by the solid curve in Fig. 28 with the best fitted values $\Delta\bar{H}_O(p) = 196 \pm 38$ kJ mol^{-1} and $\Delta\bar{H}_O(n) = -347 \pm 38$ kJ mol^{-1}, respectively, or

$$\Delta\bar{H}_O(\delta)/\text{kJ mol}^{-1}$$
$$= -(76 \pm 5) - \frac{(272 \pm 38)\delta}{[\delta^2 + (3.02 \pm 0.03) \times 10^{-11}]^{1/2}} \quad (6.11)$$

By the same argument, one can calculate $\Delta\bar{S}_O$ as

$$\Delta\bar{S}_O = \frac{n}{n+p}\Delta\bar{S}_O(n) + \frac{p}{n+p}\Delta\bar{S}_O(p)$$
$$= \left(S^o_{O_O^\times} - S^o_{V_O^{\bullet\bullet}} + S^o_p - S^o_n - \frac{1}{2}S^o_{O_2}\right)$$
$$+ R\ln\frac{(\delta + x/2)}{(3 - \delta - x/2)}$$
$$- \left(S^o_p + S^o_n - R\ln K_i\right)\frac{\beta\delta}{[(\beta\delta)^2 + 4K_i]^{1/2}}$$
$$+ R\ln\left(\frac{\beta\delta + [(\beta\delta)^2 + 4K_i]^{1/2}}{-\beta\delta + [(\beta\delta)^2 + 4K_i]^{1/2}}\right) \quad (6.12)$$

by using Eq. (5.4) or

$$\bar{S}_k = S^o_k - R\ln[k]\ (k = O_O^\times, V_O^{\bullet\bullet}, h^\bullet, e') \quad (6.13)$$

Eq. (6.12) is fitted again by using the same value $K_i = 7.41 \times 10^{33}\text{cm}^{-6}$ at 900°C to the experimental data. The result is as depicted by the solid curve in Fig. 29 with the best estimated values

$$S^o_{O_O^\times} - S^o_{V_O^{\bullet\bullet}} + S^o_p - S^o_n - \frac{1}{2}S^o_{O_2}$$
$$= 52.4 \pm 2.3\ \text{JK}^{-1}\ \text{mol}^{-1};$$
$$S^o_p + S^o_n = 865 \pm 3\ \text{JK}^{-1}\ \text{mol}^{-1} \quad (6.14)$$

or

$$\Delta\bar{S}_O(\delta)/\text{JK}^{-1}\ \text{mol}^{-1}$$
$$= (52.2 \pm 2.3) + R\ln\frac{(\delta + x/2)}{(3 - \delta - x/2)}$$
$$- \frac{(217 \pm 3)\delta}{[\delta^2 + (3.02 \pm 0.03) \times 10^{-11}]^{1/2}}$$
$$+ R\ln\left(\frac{\delta + [\delta^2 + (3.02 \pm 0.03) \times 10^{-11}]^{1/2}}{-\delta + [\delta^2 + (3.02 \pm 0.03) \times 10^{-11}]^{1/2}}\right) \quad (6.15)$$

It is pointed out that Eqs. (6.10) and (6.12) can be derived directly from Eq. (6.4) by noting that $RT\ln a_{O_2} = 2\mu_O - \mu^o_{O_2}$. Furthermore, the standard enthalpy of Reaction 6.8, $\Delta H^o(p)$ should be, in principle, equal to ΔH_{Ox} in Eq. (4.16), and similarly for Eq. (6.9), $\Delta H^o(n) = -\Delta H_{Re}$ in Eq. (2.1).

7. Concluding Remarks

For undoped $BaTiO_3$ under the isothermal condition, the basic defect chemical parameters are the densities of carriers and their mobilities: n, p, $[V_O^{\bullet\bullet}]$; u_n, u_p, D_{V_O}. Historically, authors tried to evaluate these parameters almost exclusively from the electrical conductivity isotherms. Due to the relation, Eq. (3.8), one can determine σ_n, σ_p, and σ_{ion} out of the total conductivity σ in the electron/hole/ion mixed regime or stoichiometric regime, but further analysis down to the basic parameters would be impossible without the knowledge of either mobilities or densities of the carriers. Regarding the electronic conductivity, the normal practice was to assume appropriate values for the electronic mobilities, or instead, to estimate the carrier density from the thermoelectric power via Eq. (5.9). The latter strategy, however, would be absolutely erroneous in the electron/hole/ion mixed regime, and even in the practically n-type regime, often be troublesome because the transported entropy of electrons, $\bar{S}^o_n + q^*_n/T$, remains not so well understood, see Eq. (5.6). Thermopower is, thus, practically of little use for this purpose in the electron/hole/ion mixed regime, in particular, see Eq. (5.21). It is a cross effect between charge transfer and heat transfer and, hence, more useful (and may be more logical) to evaluate the measure of the cross effect, i.e., the transported entropy or heat of transport of the carriers by using the information obtained from electrical conductivity as practiced in Section 5.

We have seen that the isothermal, chemical diffusion coefficient supplements the electrical conductivity in the mixed regime. From the chemical diffusivity, one determines $\tilde{D}^o$ (Eq. (4.8)) and $a^o_{O_2}$ (Eq. (2.13)) via Eq. (4.7), which in association with σ_{ion}, $\sigma_{el,m}$ (Eq. (3.1)) and $a^*_{O_2}$ (Eq. (3.7)) lead to the evaluation of u_n and u_p separately. Then, electron density "n" is unequivocally evaluated against oxygen activity, which in association with charge neutrality condition, Eq. (2.8), or Eq. (4.11), leads to the evaluation of $[V_O^{\bullet\bullet}]$ in the mixed regime. The latter subsequently allows one to determine D_{V_O} from σ_{ion} via Eq. (3.4).

The nonstoichiometry, δ, is equivalent to the chemical diffusivity in terms of defect-chemical information content: One can also determine both K_i and $a^o_{O_2}$ due to Eq. (6.4) in the mixed regime. In this sense, the nonstoichiometry information is redundant in principle. The latter may, thus, be profitably employed to confirm the accuracy or inter-consistency of the basic parameters evaluated from σ and $\tilde{D}$.

The authors have pursued this strategy with the "undoped" $BaTiO_3$. To our dismay, though, it has turned out that even though the variation of the nonstoichiometry against oxygen partial pressure, Fig. 24, looks consistent with the corresponding conductivity (Fig. 4), chemical diffusivity (Fig. 10) and thermopower (Fig. 20), it is not quite so in detail as is demonstrated in Figs. 25 and 26.

It is again reminded that the specimens for the nonstoichiometry measurement was prepared from nominally the same starting powder (99.995% purity) of those for the measurement of conductivity, chemical diffusivity and thermopower. The only formal difference is with their microstructures: the latter are of $94 \pm 1\%$ dense with a grain size of 43 ± 8 μm; the former ca. 90% dense with 60 ± 20 μm grains, but this difference seems to be too small to speak of the microstructural effect on nonstoichiometry. Considering the formal similarity in purity and microstructure of all those specimens, therefore, the discrepancy between the nonstoichiometry result and the chemical diffusivity result is hard to understand. It may then be noted that while the specimens for conductivity, chemical diffusivity and thermopower were cut out of the identical cake of sintered $BaTiO_3$, those for nonstoichiometry were from the other one that had been prepared much later at different place. We thus suspect that this discrepancy may be attributed to the possibility that extents of impurity pick-up during processing at elevated temperatures was different even though the

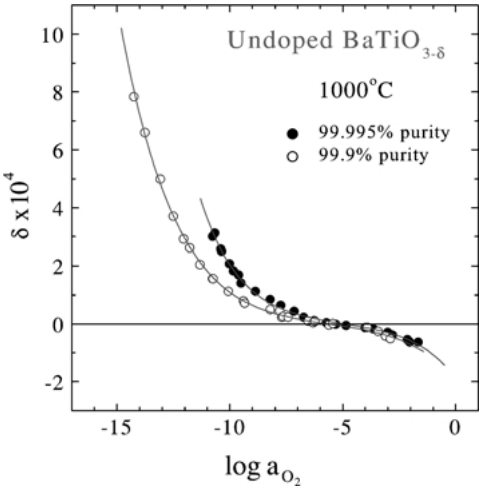

Fig. 30. Oxygen nonstoichiometry depending on nominal purity of undoped $BaTiO_{3-\delta}$, 99.9% (○) and 99.995%(●) purity of starting powder, respectively.

starting powder purity had been originally the same. One circumstantial evidence supporting this suspicion is shown in Fig. 30, where the nonstoichiometry of "undoped" $BaTiO_3$ with a nominal purity of 99.9% is compared with that of 99.995% purity in Fig. 24. Obviously, the nonstoichiometries differ depending on the nominal purities: Detailed analysis[5] shows that at the temperature of comparison, 1000°C, the 99.9% pure sample has the values, $\log (K_i/\text{cm}^{-6}) = 35.02 \pm 0.07$ and $\log a^o_{O_2} = -5.7 \pm 0.2$, while the 99.995% one $\log (K_i/\text{cm}^{-6}) = 35.08 \pm 0.04$ and $\log a^o_{O_2} = -4.94 \pm 0.08$. The present situation is reminiscent of a classical wisdom in defect chemical study of ceramics at elevated temperatures: All measurements be done on an identical specimen in the shortest possible time. Whatever the exact cause for the discrepancy is, we believe that at least, the first three transport properties, electrical conductivity, chemical diffusivity and thermopower remain consistent with each other because the specimens are from an identical bulk of $BaTiO_3$.

Even though the defect parameters K_i and $a^o_{O_2}$ evaluated from the nonstoichiometry are not in good agreement with those from the chemical diffusivity, we can still get an insight into the correlation of the transport properties with the absolute nonstoichiometry. In Fig. 31(a)–(c), we plot against oxygen nonstoichiometry, as determined in Fig. 24, the electrical conductivity, the thermoelectric power and the chemical diffusivity. One can notice clear correspondences. Noting that at 1000°C in particular, the $\log a^o_{O_2}$-value ($= -4.94$) as

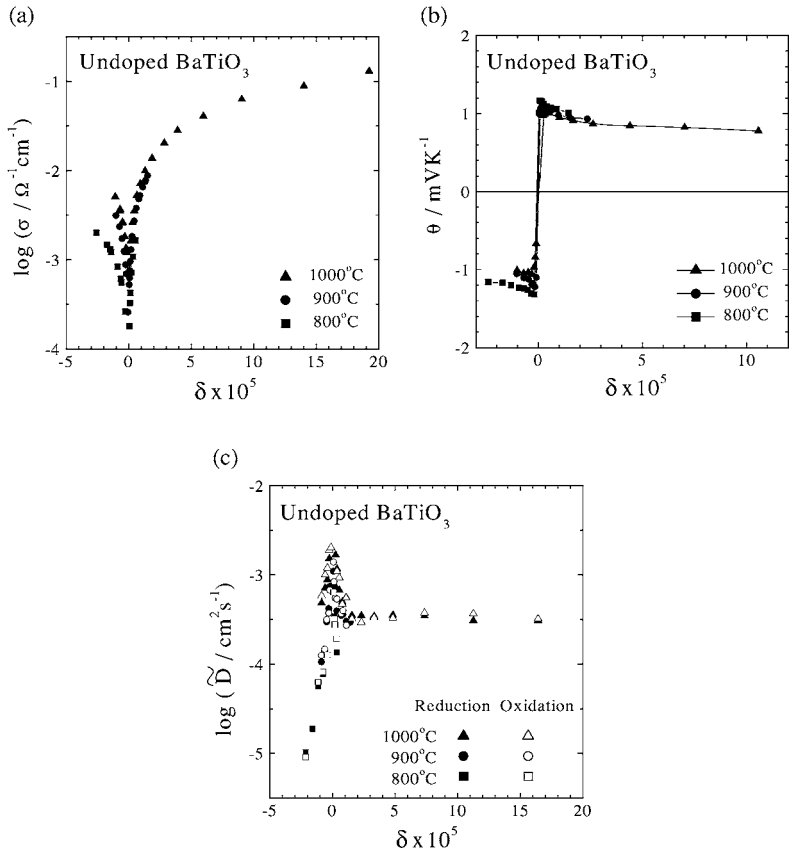

Fig. 31. Correlation of the transport properties with the absolute nonstoichiometry; (a) electrical conductivity, (b) thermopower, (c) chemical diffusivity, respectively, vs. oxygen nonstoichiometry.

determined from δ is sufficiently close to that ($=-5.14$) as determined from $\tilde{D}$, one can see again that a drastic change in each transport property occurs crossing approximately the electronic stoichiometric composition $\delta \equiv 0$ (or $n \equiv p$): The conductivity becomes minimum upon switching from a p-type ($\delta < 0$) branch to an n-type branch ($\delta > 0$), accordingly the thermopower changes its sign and the chemical diffusivity becomes maximum. One should be aware, however, that this is not always the case; this is only because the mobility ratio is not far from one ($b = 1.6$) for the present system of undoped $BaTiO_3$.

In retrospect, the defect structure of $BaTiO_3$was first grounded on electrical conductivity measurement. Now by adding the information on chemical diffusivity as a measure of nonstoichiometry equilibration kinetics, one has been able to draw a more precise, collective, and consistent picture on the defect structure. Nevertheless, there still remains enigmatic the identity of the effective acceptors A' the concentration of which is thermally activated for the "undoped" $BaTiO_3$ (Eq. (4.12)). The answers to the remaining questions concerning the defect structure of undoped $BaTiO_3$ seems to hinge very much on the identity of these acceptors.

List of Symbols

a_{O_2}, activity of gas oxygen ($\equiv P_{O_2}/\text{atm}$)
$a^o_{O_2}$, oxygen activity corresponding to $n = p$
$a^*_{O_2}$, oxygen activity corresponding to $\sigma_n = \sigma_p$
a_{BaO}, activity of BaO
b, electrochemical mobility ratio of electrons to holes ($= u_n/u_p$)
D_O, self diffusion coefficient of oxide ions
D_{V_O}, diffusion coefficient of oxygen vacancies
$\tilde{D}$, chemical diffusion coefficient of component oxygen
e, elementary charge

$\Delta\bar{G}_{\mathrm{O}}$, relative partial molar Gibbs free energy of component oxygen
$\bar{H}_k$, partial molar enthalpy of species k
H_k^o, standard molar enthalpy of species k
ΔH_A, activation enthalpy of [A′]
ΔH_g^o, standard enthalpy of the reaction, $\mathrm{CO} + \frac{1}{2}\mathrm{O}_2 = \mathrm{CO}_2$
ΔH_i, enthalpy of intrinsic electronic excitation reaction (= thermal band gap)
ΔH_j the enthalpy change of the relevant reaction j
ΔH_{Ox}, enthalpy of oxidation reaction
ΔH_{Re}, enthalpy of reduction reaction
ΔH_S, Schottky defect formation enthalpy
$\Delta\bar{H}_{\mathrm{O}}$, relative partial molar enthalpy of component oxygen
$\Delta\bar{H}_{\mathrm{O}}(n)$, relative partial molar enthalpy of oxygen in the n-type branch
$\Delta H_{\mathrm{O}}^o(n)$, standard enthalpy of oxygen in the n-type branch
$\Delta\bar{H}_{\mathrm{O}}(p)$, relative partial molar enthalpy of oxygen in the p-type branch
$\Delta H_{\mathrm{O}}^o(p)$, standard enthalpy of oxygen in the p-type branch
k, Boltzmann constant
K_B, equilibrium constant for BaO incorporation
K_i, intrinsic electronic excitation equilibrium constant
K_j, equilibrium constant for reaction j(= S, B, i, Ox, Re)
K_j^o, pre-exponential factor of K_j
K_{Ox}, oxidation equilibrium constant
K_{Re}, reduction equilibrium constant
K_{Re}^o, pre-exponential factor of K_{Re}
K_S, schottky equilibrium constant
m, oxygen exponent of concentration of holes ($+m$) or electrons ($-m$)
n, concentration of free electrons
N_A, Avogadro's number
p, concentration of electron holes
P_{CO}, partial pressure of CO
P_{CO_2}, partial pressure of CO_2
P_{O_2}, oxygen partial pressure
q_k^*, reduced heat-of-transport of species k
R, gas constant
r, mixing ratio CO_2 to CO (= $P_{\mathrm{CO}_2}/P_{\mathrm{CO}}$)
$\bar{S}_k$, partial molar entropy of species k
$\bar{S}_k^o$, standard molar entropy of species k
$S_{\mathrm{O}_2}^o$, standard entropy of gas oxygen
$S_{\mathrm{CO}_2}^o$, standard entropy of gas CO_2
S_{CO}^o, standard entropy of gas CO
$\Delta\bar{S}_{\mathrm{O}}$, relative partial molar entropy of component oxygen
T, absolute temperature
t_{el}, electronic transference number
t_{ion}, ionic transference number (= $1 - t_{\mathrm{el}}$)
u_k, electrochemical mobility of species k
V_m, molar volume of BaTiO_3
$W = (\frac{\partial\mu_{\mathrm{O}}}{\partial\delta})_T \frac{d\delta}{dT}$, thermodynamic factor
x, site fraction of the effective acceptors A′.
α, conductivity ratio of holes to electrons (= σ_p/σ_n)
δ, oxygen deficit or nonstoichiometry of $\mathrm{BaTiO}_{3-\delta}$
δ^*, initial nonstoichiometry of $\mathrm{BaTiO}_{3-\delta}$
$\Delta\delta$, nontoiciometry difference for each titration run (= $\delta - \delta^*$)
η_k, electrochemical potential of species k
θ, absolute thermoelectric power
θ_{el}, thermopower by electrons as a charged component (building unit)
θ_{ion}, thermopower by mobile ions as a charged component (building unit)
θ_n, thermopower by electrons as a defect
θ_p, thermopower by holes as a defect
μ_k, chemical potential of species k(= n, p, O, O_2, CO_2, CO)
$\mu_{\mathrm{O(S)}}$, chemical potential of component oxygen in the solid phase
$\mu_{\mathrm{O}_2(\mathrm{g})}$, chemical potential of oxygen molecule in the gas phase
$\mu_{\mathrm{O}_2(\mathrm{g})}^o$, standard chemical potential of gas oxygen
ξ, nonmolecularity such as $\mathrm{Ba}_{1+\xi}\mathrm{TiO}_{3+\delta}$
σ, total conductivity
σ_{el}, electronic conductivity
$\sigma_{\mathrm{el},m}$, minimum electronic conductivity
σ_k, partial conductivity of species k
Indices (k)
- O, oxygen as a chemical component
- O^{2-}, oxide ion as a charged component
- ion, ion as a mobile charged component (=O^{2-} in the present context)
- el, electron as a charged component
- n, carrier electrons
- p, carrier holes
- V_{O}, oxygen vacancy

Acknowledgments

This work was financially supported by the Center for Advanced Materials Processing under the "21C

Frontier Program" of Ministry of Science and Technology, Korea.

Notes

1. A lattice molecule of the present system should, thus, be rigorously represented as $Ba_{1+\xi}TiO_{3-\delta}$, where ξ denotes the (cation) nonmolecularity as a measure of Ba-excess relative to Ti-content and δ the (oxygen) nonstoichiometry as a measure of oxygen deficit. Nevertheless, we will eventually assume in this article that ξ remains practically fixed for kinetic reasons (or cation sublattices are closed) and only the nonstoichiometry is changing due to the redox equilibrium, Eq. (2.1).
2. In this article, we often call this region the stoichiometric regime becasuse $[V_O^{\bullet\bullet}]$ is practically fixed and hence, $\delta \approx 0$, see Eq. (6.1).
3. This implies that oxygen exchanges only with the already existing oxygen vacancies ($[V_O^{\bullet\bullet}] \approx [A']/2$), and the cation sublattices or $[A']$ remain fixed irrespective of oxygen activity at a given temperature. Therefore, the internal equilibrium of Eq. (2.4) may not necessarily be achieved in the rigorous sense.
4. The specimens of the authors' own were of a bar shape measuring 2.15 mm × 2.15 mm × 14.7 mm.
5. As the oxygen partial pressure range examined for the 99.9% pure specimen extends partially to the disorder regime of (n, $V_O^{\bullet\bullet}$) in Fig. 2, the nonstoichiometry change as measured has been fitted to Eq. (6.3) as depicted by the solid curve in Fig. 30. [13]

References

1. B.M. Kulwicki, in *Grain Boundary Phenomena in Electronic Ceramics, Advances in Ceramics*, vol. 1, edited by L.M. Levinson (Am. Ceram. Soc., Columbus, Ohio, 1981), p. 138.
2. G. Goodman, in *Grain Boundary Phenomena in Electronic Ceramics*, op. cit., p. 215.
3. A.I. Kingon, S.K. Streiffer, C. Basceri, and S.R. Summerfelt, *MRS Bulletin*, 46 (1996).
4. J.F. Scott, *Ferroelectrics Review*, **1**, 1 (1998).
5. R. Wernicke, *Phys. Stat. Sol.* (a), **47**, 139 (1978).
6. A.Z. Hed and D.S. Tannhauser, *J. Chem. Phys.*, **47**, 2090 (1967).
7. J. Yahia, *Phys. Rev.*, **130**, 1711 (1963).
8. J. Nowotny, M. Radecka, and M. Rekas, *J. Phys. Chem. Solids*, **58**, 927 (1997).
9. C.-R. Song and H.-I. Yoo, *Solid State Ionics*, **120**, 141 (1999).
10. C.-R. Song and H.-I. Yoo, *Phys. Rev.* B, **61**, 3975 (2000).
11. C.-R. Song and H.-I. Yoo, *Solid State Ionics*, **124**, 289 (1999).
12. H.-I. Yoo and C.-R. Song, *J. Electroceram.*, **6**, 61 (2001).
13. D.-K. Lee and H.-I. Yoo, *Solid State Ionics*, **144**, 87 (2001).
14. C.-R. Song and H.-I. Yoo, *J. Am. Ceram. Soc.*, **83**, 773 (2000).
15. F.D. Morrison, A.M. Coast, D.C. Singlair, and A.R. West, *J. Electroceram.*, **6**, 219 (2001).
16. J.-Y. Kim, C.-R. Song, and H.-I. Yoo, *J. Electroceram.*, **1**, 27 (1997).
17. J. Nowotny and M. Rekas, *Solid State Ionics*, **49**, 135 (1991).
18. G.V. Lewis and C.R.A. Catlow, *Radiat. Effects*, **73**, 307 (1983).
19. D.-K. Lee and H.-I. Yoo, *Solid State Ionics*, in press.
20. J. Maier, *J. Am. Ceram. Soc.*, **76**(5), 1212 (1993).
21. J. Maier, *ibid.*, **76**, 1223 (1993).
22. J.F. Baumard and P. Abelard, *Solid State Ionics*, **12**, 47 (1984).
23. V.V. Prisedskii and Yu. D. Tret'yakov, *News. Acad. Sci. USSR, Inorg. Mater.*, **18**(2), 1659 (1982).
24. N.G. Eror and D.M. Smyth, *J. Solid State Chem.*, **24**, 235 (1978).
25. N-H. Chan and D.M. Smyth, *J. Electrochem. Soc.*, **123**(10), 1584 (1976).
26. N-H. Chan, R.K. Sharma, and D.M. Smyth, *J. Am. Ceram. Soc.*, **64**(9), 556 (1981).
27. S.A. Long and R.N. Blumenthal, *J. Am. Ceram. Soc.*, **54**, 515 (1971).
28. A.M.J.H. Seuter, *Philips Res. Repts. Suppl.*, **3**, 1 (1974).
29. J. Daniels and K.H. Härdtl, *Phil. Res. Repts.*, **31**, 489 (1976).
30. J. Nowotny and M. Rekas, *Ceram. Int.*, **20**, 225 (1994).
31. J. Nowotny and M. Rekas, *J. Europ. Ceram. Soc.*, **5**, 173 (1989).
32. S.A. Long and R.N. Blumenthal, *J. Am. Ceram. Soc.*, **54**, 577 (1971).
33. J.H. Becker and J.P.R. Frederikse, *J. Appl. Phys.*, **33**(1), 447 (1962).
34. H.-I. Yoo and C.-S. Kim, *Solid State Ionics*, **53–56**, 583 (1992).
35. R. Wernicke, *Philips Res. Rep.*, **31**(6), 489 (1976).
36. J. Maier, G. Schwitzgebel, and H.-J. Hagemann, *J. Solid State Chem.*, **58**, 1 (1985).
37. A. Müller and K.H. Härdtl, *Appl. Phys.* A, **49**, 75 (1989).
38. J. Nowotny and M. Rekas, *Ceram. International*, **20**, 265 (1994).
39. S. Shirasaki, H. Yamamura, H. Haneda, K. Kakegawa, and J. Moori, *J. Chem. Phys.*, **73**, 4640 (1980).
40. S. Shirasaki, H. Haneda, K. Arai, and M. Fujimoto, *J. Mat. Sci.*, **22**, 4439 (1987).
41. A. Garcia-Verduch and R. Linder, *Arkiv Kemi*, **5**, 313 (1953).
42. K.D. Becker, H. Schmalzried, and V. von Wurmb, *Solid State Ionics*, **11**, 213 (1983).
43. W. Sitte, *Solid State Ionics*, **94**, 85 (1997).
44. C. Wagner, *Z. Phys. Chem.* B, **21**, 25 (1933).
45. T. Bieger, J. Maier, and R. Waser, *Sensors and Actuators* B, **7**, 763 (1992).
46. J. Claus, I. Denk, M. Leonhardt, and J. Maier, *Ber. Bunsenges. Phys. Chem.*, **101**, 1386 (1997).
47. N.-H. Chan, R.K. Sharma, and D.M. Smyth, *J. Am. Ceram. Soc.*, **65**, 167 (1982).
48. J. Nowotny and M. Rekas, *Ceram. International*, **20**, 257 (1994).
49. H.-J. Hagemann and D. Hennings, *J Am. Ceram. Soc.*, **64**, 590 (1981).
50. H.-I. Yoo and C.-R. Song, *Electrochemistry*, **68**(6), 415 (2000).
51. C.-S. Kim and H.-I. Yoo, *J. Electrochem. Soc.*, **143**, 2863 (1996).
52. C.-S. Kim and H.-I. Yoo, *Korean J. Ceram.*, **14**(2), 151 (1998).
53. D.-K. Lee and H.-I. Yoo, *J. Electrochem. Soc.*, **147**, 2835 (2000).
54. B. Ma, U. Balachandran, J.-H. Park, and C.U. Segre, *ibid.*, **143**(5), 1736 (1996).
55. R.M. Waser, *J. Am. Ceram. Soc.*, **72**(12), 2234 (1989).
56. J. Blanc and D.L. Staebler, *Phys. Rev.* B, **4**(10), 3548 (1971).
57. S.K. Mohapatra and S. Wagner, *J. Appl. Phys.*, **50**(7), 5001 (1979).
58. P. Gerthsen, R. Groth, and K.H. Härdtl, *Phys. Stat. Sol.*, **11**, 303 (1965).
59. J. Mizusaki, T. Sasamoto, W.R. Cannon, and H.K. Bowen, *J. Am. Ceram. Soc.*, **65**(8), 363 (1982).

60. J. Mizusaki, T. Sasamoto, W.R. Cannon, and H.K. Bowen, *J. Am. Ceram. Soc*., **66**, 247 (1983).
61. L.-W. Tai, M.M. Nasrallah, and H.U. Anderson, *J. Solid State Chem*., **118**, 117 (1995).
62. G.H. Jonker, *Philips. Res. Repts.*, **23**, 131 (1968).
63. C. Jones, P.J. Grout, and A.B. Lidiard, *Phil. Mag.* A, **79**, 2051 (1999).
64. C. Wagner, *Prog. Solid State Chem.*, **7**, 1 (1972).
65. H.-I. Yoo, D.-S. Sinn, and J.-O. Hong, *J. Electrochem. Soc*., **145**(3), 1008 (1998).
66. H.-I. Yoo and J.-H. Whang, *J. Phys. Chem. Solids*, **53**(7), 973 (1992).
67. D.R. Gaskell, in *Introduction to the Thermodynamics of Materials*, 3rd edn. (Taylor & Francis, Washington, DC, 1995), p. 544.
68. C. Korte and J. Janek, *J. Phys. Chem. Solids*, **58**(4), 623 (1997).
69. G.V. Bois, N.A. Mikhailova, E.I. Prodavtsova, and V.A. Yusova, *News. Acad. Sci. USSR, Inorg. Mat*., **12**, 1302 (1976).
70. R.J. Panlener and R.N. Blumenthal, *J. Am. Ceram. Soc*., **54**, 610 (1971).
71. D. Hennings, *Phil. Res. Repts.*, **31**, 516 (1976).
72. C. Wagner, *Prog. Solid State Chem.*, **6**, 1 (1971).
73. H. Ihrig, *J. Phys. C*, **9**, 3469 (1976).